


RESEARCH ARTICLE | FEBRUARY 06 2025

# Multiscale pore structure characteristics of deep marine shale and its control on the gas transport mode

Shijie He (贺世杰) ; Pingping Li (李平平); Zhenxue Jiang (姜振学); Xianglu Tang (唐相路)*Physics of Fluids* 37, 026608 (2025)<https://doi.org/10.1063/5.0251571>

## Articles You May Be Interested In

Heterogeneity properties and permeability of shale matrix at nano-scale and micron-scale

*Physics of Fluids* (September 2024)

Machine learning method for shale gas adsorption capacity prediction and key influencing factors evaluation

*Physics of Fluids* (January 2024)

Slickwater residues in shale multi-scale pore structures

*Physics of Fluids* (December 2024)

Physics of Fluids

## Special Topics Open for Submissions

[Learn More](#)

# Multiscale pore structure characteristics of deep marine shale and its control on the gas transport mode

Cite as: Phys. Fluids **37**, 026608 (2025); doi: [10.1063/5.0251571](https://doi.org/10.1063/5.0251571)

Submitted: 3 December 2024 · Accepted: 5 January 2025 ·

Published Online: 6 February 2025



View Online



Export Citation



CrossMark

Shijie He (贺世杰),<sup>1,2,a)</sup>  Pingping Li (李平平),<sup>1,2</sup> Zhenxue Jiang (姜振学),<sup>1,3</sup> and Xianglu Tang (唐相路)<sup>1,3</sup>

## AFFILIATIONS

<sup>1</sup>National Key Laboratory of Petroleum Resources and Engineering, China University of Petroleum (Beijing), Beijing 102249, China

<sup>2</sup>College of Geosciences, China University of Petroleum (Beijing), Beijing 102249, China

<sup>3</sup>The Unconventional Oil and Gas Institute, China University of Petroleum (Beijing), Beijing 102249, China

<sup>a)</sup>Author to whom correspondence should be addressed: [hsjcupb@163.com](mailto:hsjcupb@163.com)

## ABSTRACT

Deep marine shale has undergone intricate geological evolution, with pore development at the nanoscale. Consequently, quantifying the impact of the pore structure on gas is challenging. In this paper, the microscopic space structure of deep shale was quantified, and the correlation between the pore structure and the mode of gas transport was established. This study focused on the Silurian Longmaxi Formation shale, using experimental testing and fractal dimension methods to quantify pore characteristics and control factors at multiscale, and establishing the relationship between pore structure and gas transport mechanism. The results indicated that the main lithofacies are organic-rich siliceous shale and organic-rich mixed shale. The preservation of pores by siliceous minerals and high pressure is the key to the high-quality reservoir. Based on gas transport mechanisms, there are five types of gas transport modes: surface adsorption-diffusion, Knudsen diffusion, Fick diffusion, slip flow, and continuous flow. The critical pore size was 1.2, 4.34, 15, and 180 nm, respectively. Compared to shallow shale, the abundance of micropores and mesopores in deep shale is greater, and the contribution of microfractures to shallow shale gas transport is crucial. In conclusion, favorable exploration in targeting organic-rich siliceous shale with low  $D_1$  and high  $D_2$ , as well as organic-rich mixed shale segments with high  $D_1$  and high  $D_2$ . Specifically, within hydrocarbon-rich basins located below 3500 m, it is recommended to search for overpressure regions with weak structural deformation. This research establishes a basis for the exploration and geological principles of deep marine shale.

Published under an exclusive license by AIP Publishing. <https://doi.org/10.1063/5.0251571>

## I. INTRODUCTION

As exploration and development technologies progress, abundant natural gas reservoirs within shale formations have garnered significant interest.<sup>1</sup> In recent years, shale gas production has increased significantly and has emerged as a vital alternative energy source.<sup>2,3</sup> Shale gas, located in the micropores/nanopores of organic-rich black shale, exists in both adsorbed and free states.<sup>4</sup> The features of pore structure directly govern the enrichment, state of occurrence, and transportation of gas. Systematic research on micro-structure has both theoretical and practical significance.<sup>2,4,5</sup> Due to the demand for exploration of natural gas, shale presents challenges in testing and characterization due to its complex pore structures. It has become a hot topic of shale pores to quantitatively characterize nano-scale features that cannot be obtained by experiment using mathematical simulation methods.<sup>6–8</sup>

The deep marine shale pores that have experienced complex geological evolution are concentrated at the nanoscale. Due to the limited size of small-scale shale pores, characterizing the pore structure and quantifying the influence of the pore structure on gas are challenging.<sup>7–10</sup> Currently, there are notable challenges in the field of pore structure research. The integration of quantitative testing and qualitative observations of pores remains limited.<sup>11,12</sup> It is difficult to establish a correlation between shale pore structure parameters and gas transport modes.<sup>13–15</sup> Furthermore, there is a lack of characterization and quantification methods for certain shale features that cannot be directly tested, such as the spatial distribution of structures.<sup>16–18</sup> Moreover, the spatial arrangement of shale pores exhibits notable heterogeneity and is recognized as a key factor influencing the transport mechanism of gas. In the characterization of shale pores, employing

scanning electron microscope (SEM) for the study of microscopic pores provides a research approach for the direct imaging of pores.<sup>7,19</sup> Techniques involving fluid injection have the ability to acquire parameters related to pore structure, facilitating the characterization of permeable pores.<sup>20–22</sup> Fractal modeling based on N<sub>2</sub> adsorption data allows quantitative descriptions of the structural features of porous media,<sup>23</sup> thus providing a fundamental basis for correlating gas transport modes with pore structures.<sup>24</sup> These methodologies have become crucial methods in the study of pores.<sup>4,9,25,26</sup> At present, the deep marine organic-rich shale gas in the Sichuan Basin is receiving increasing attention.<sup>27</sup> The burial depth of the main producing layers in North America rarely exceeds 3500 m, and there is little experience in terms of deep shale gas exploration and development.<sup>28,29</sup> Furthermore, comprehensive investigations concerning the pore structure and mode of gas transport in deep shale are lacking.

In this paper, the Silurian Longmaxi Formation shale in the southern Sichuan Basin is investigated as the research target. Rock cores from the Luzhou and Changning areas were selected as experimental samples. A comprehensive approach combining total organic carbon (TOC), X-ray diffraction (XRD), SEM observation, High Pressure Mercury Intrusion (HPMI) experiments, and CO<sub>2</sub> and N<sub>2</sub> adsorption tests was employed to reveal the following points. (1) The development characteristics and mechanism of pore structure of deep marine shale are expounded. (2) Based on Knudsen number and adsorption mechanism, the main types and critical conditions of deep shale gas diffusion and seepage are clarified. (3) By comparing the pore structure of deep and shallow marine shale, the reasons restricting the exploration of deep shale are analyzed.

## II. GEOLOGIC SETTING

The Changning and Luzhou blocks are located in the southern region of the Sichuan Basin and are positioned between the Longmenshan fold belt, the Emeishan-Liangshan fold belt, and the Hunan-Guizhou-Hubei fold belt.<sup>30</sup> During the initial deposition of the Longmaxi Formation, the sedimentary setting in the study region predominantly featured muddy semideep to deep-water shelf conditions, alongside calcareous semideep to deep-water shelf facies.<sup>31,32</sup> These environments created strong reducing conditions, promoting the conservation of ample organic matter (TOC > 2%). The organic matter is mainly composed of sapropelic and mixed-type kerogens (type I and type II).<sup>33,34</sup> The shale comprises a substantial proportion of fragile minerals (>40%), and the lithofacies are primarily composed of organic-rich siliceous and mixed shale lithofacies. These have higher hydrocarbon generation capacities and degrees of thermal evolution (Ro > 2.0%).<sup>35</sup> In the later stages of Longmaxi Formation deposition, as the sea level decreased and the terrigenous clastic supply intensified,<sup>36</sup> the sedimentary environment transitioned to a shallow to sub-aqueous shelf.<sup>37</sup> This shift led to a reduction in organic matter abundance and an increase in clay content. The lithofacies prevalent in this period were characterized primarily by clay-rich shale lithofacies and calcareous shale lithofacies.<sup>38–40</sup>

## III. SAMPLES AND ANALYTICAL METHODS

In this study, a total of 36 Lower Silurian Longmaxi Formation black shale samples were selected from five wells in southern Sichuan. The location of the well is shown in Fig. 1. Most of the shale samples used by were collected from the bottom and middle-lower parts of the Longmaxi Formation. Among them, 36 samples were subjected to

TOC and XRD experiments, and 21 samples were subjected to CO<sub>2</sub> adsorption, N<sub>2</sub> adsorption, and HPMI experiments. SEM experiments were carried out on 10 samples.

For the analysis of shale petrological components, TOC and XRD test experiments were carried out. First, the samples were dried at low temperature and ground to more than 80 mesh. Subsequently, the sample was acid-washed with excess hydrochloric acid for 3 h, and then washed with distilled water until it reached neutral. Finally, the samples were baked at low temperature until completely dried for TOC content test. The samples were ground to more than 200 mesh for XRD experiments.

For the shale reservoir characterization experiment, the samples were first subjected to argon ion grinding for 2 h, and then SEM experiments were performed to observe the pore type. The pore structure parameters were obtained by using CO<sub>2</sub> adsorption, N<sub>2</sub> adsorption, HPMI experiments, and combining the Brunauer–Emmett–Teller (BET), Barrett–Johner–Halenda (BJH) models, and density functional theory (DFT) model.<sup>41,42</sup> These are used to quantitatively characterize the microscopic development characteristics of shale pores.

There are many methods to calculate the fractal dimension of solids based on gas adsorption-desorption isotherm. The fractal dimension is introduced into the adsorption potential theory when studying the adsorption of gas molecules on porous solids with heterogeneous surfaces.<sup>43,44</sup> The gas adsorption model on the fractal surface in the capillary condensation region is established, namely the Frenkel–Halsey–Hill (FHH) equation, as follows:

$$\ln V = \text{Const} + (D - 3) \times \ln \left( \ln \frac{P_0}{P} \right), \quad (1)$$

where V is the gas adsorption capacity (cm<sup>3</sup>/g); P is the system equilibrium pressure (MPa); P<sub>0</sub> is the saturated vapor pressure of the adsorbed gas (MPa); Const is a constant; D is the fractal dimension of the porous material, and the value of D is between 2 and 3. The larger the fractal dimension, the rougher the surface of the material.

## IV. RESULTS

### A. Classification of lithofacies

The shale is mainly a fine-grained sedimentary record in a weak hydrodynamic environment, and its sedimentary structure is simple. Different rock facies show different characteristics in mineral composition, paleontology, organic matter enrichment, and logging response. Multiple factors control the formation of shale gas sweet spots.<sup>45</sup> This paper believes that reasonable lithofacies division needs to focus on key factors such as shale petrology and sedimentary environment (i.e., genesis) and can reflect the typical rock types of shale strata. Based on the sampling analysis and test of the key exploration wells of Longmaxi Formation in southern Sichuan, the quantitative classification standard of lithofacies types based on quartz, clay, and carbonate minerals and combined with organic matter content was established.

In this study, we utilize the categorization framework introduced by Tang *et al.*,<sup>46</sup> which relies on mineral composition and organic matter content, to classify shale lithofacies. According to the TOC content, shale can be categorized into three groups: those exceeding 2% TOC are labeled organic-rich shale, those with TOC contents ranging between 1% and 2% are termed organic-fair shale, and those with TOC contents below 1% are designated organic-poor shale. Based on variations in mineral composition, shale can be categorized into four

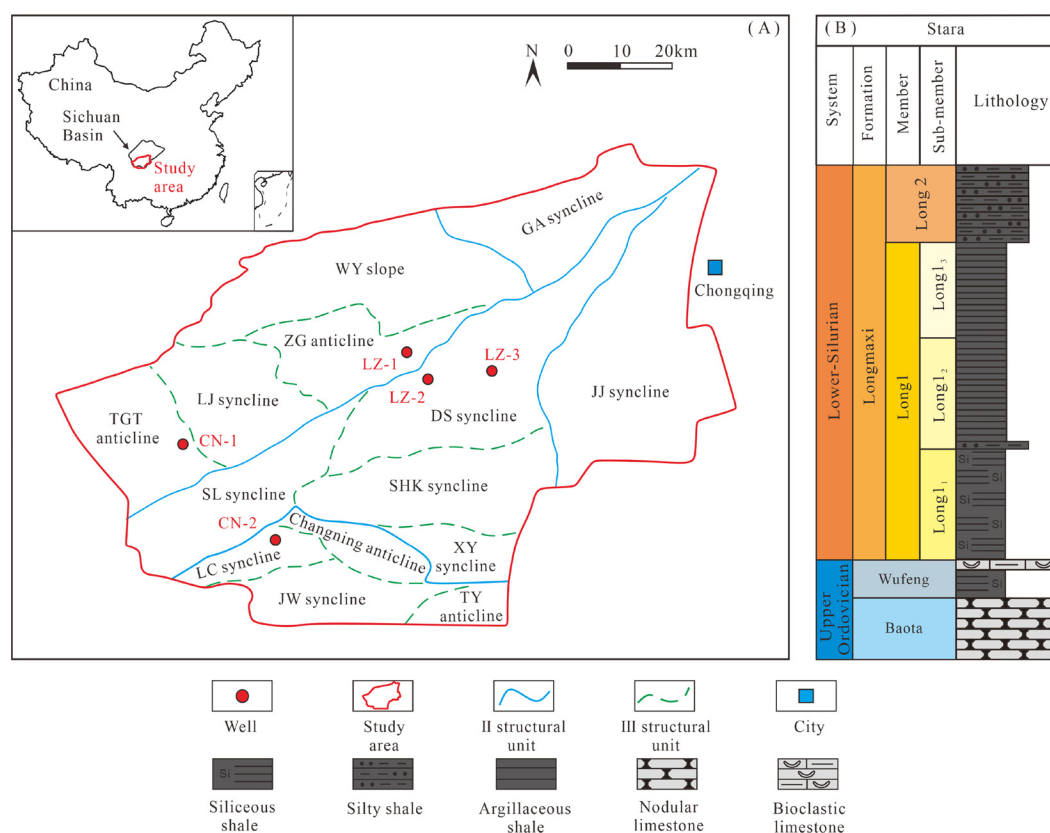


**FIG. 1.** Sample location map of the Sichuan basin and stratigraphic column of study strata. (a) Sampling well location and geological background of the Sichuan Basin and southern Sichuan area. (b) Stratigraphic sequence of the Longmaxi Formation of the lower-Silurian.

groups: argillaceous shale (I, clay  $\geq 40\%$ ), calcareous shale (II,  $\text{Ca/Si} \geq 2$ ), mixed shale (III, clay minerals  $< 40\%$ ,  $1/2 \leq \text{Ca/Si} < 2$ ), and siliceous shale (IV, clay  $< 40\%$ ,  $\text{Ca/Si} < 1/2$ ). Based on the combined mineral composition and TOC content, shale lithofacies can be categorized into 12 groups: organic-rich argillaceous shale (ORAS), organic-rich siliceous shale (ORSS), organic-rich mixed shale (ORMS), organic-rich calcareous shale (ORCS), organic-fair argillaceous shale (OFAS), organic-fair siliceous shale (OFSS), organic-fair mixed shale (OFMS), organic-fair calcareous shale (OFCS), organic-poor argillaceous shale (OPAS), organic-poor siliceous shale (OPSS), organic-poor mixed shale (OPMS), and organic-poor calcareous shale (OPCS) (Fig. 2).

As depicted in Table I, organic-rich shale samples in the southern Sichuan region are primarily distinguished by argillaceous and siliceous lithofacies in the Luzhou block, whereas the Changning block is predominantly composed of mixed lithofacies shale. The lithofacies classification results closely align with previous studies on the lithofacies classification of the Longmaxi Formation shale.<sup>45,47</sup> This similarity indicates that the selected samples are representative in nature.

## B. Pore types and morphological characteristics

Pore type and structure serve as pivotal elements in assessing shale reservoir quality. Currently, there is no unified classification

scheme for shale pores. In this study, a categorization framework,<sup>48</sup> organic matter pores (OM pores), inorganic pores (intragranular pores and intergranular pores), and microfractures are used.

A substantial number of OM pores are present in the deeper strata of the Longmaxi Formation shale in the southern Sichuan Basin. The pore width ranges from nanometers to micrometers. Due to the different contact relationships between the location of organic matter and surrounding minerals, the development forms of OM pores are different. Most of them are irregular in shape, with nanolevel sponge shapes and micrometer-level bubble holes.

Organic matter and clay minerals are symbiotic and distributed parallel to the clay layer in the form of long strips. The OM pores are irregular or elliptical, with uneven pore widths [Fig. 3(a)]. Clay minerals are strongly deformed due to extrusion, resulting in highly irregular internal OM pores with a wide range of pore width variations [Figs. 3(b) and 3(c)]. Honeycomb-shaped OM pores are predominantly distributed within isolated or banded organic matter structures and exhibit elliptical or nearly circular shapes. These OM pores exhibit a high degree of heterogeneity at multiple scales [Fig. 3(d)]. The sponge-like OM pores are developed around some of the OM pores [Fig. 3(e)], forming a network of interconnected pores. In this way, the pores significantly enhance connectivity, resulting in hydrocarbon accumulation. Some of the organic matter does not develop pores or develops



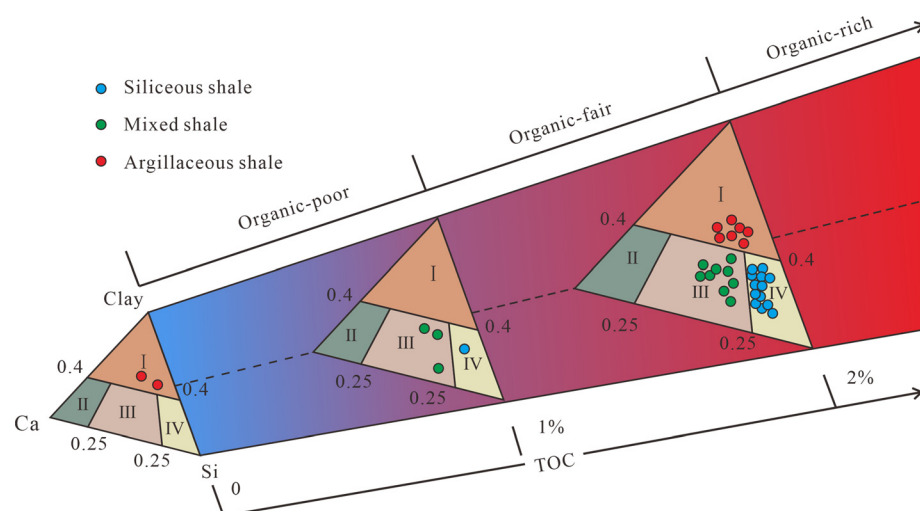


**FIG. 2.** Categorization of lithofacies in deep marine shale. Si: Siliceous minerals, mainly quartz; Ca: carbonates, mainly comprising calcite and dolomite; Clay: clay minerals. I: argillaceous shale; II: calcareous shale; III: mixed shale; IV: siliceous shale.

locally, which can be observed in irregular agglomerated organic matter [Fig. 3(f)] and may be related to the type of organic matter. In addition, the Longmaxi Formation experienced a strongly reducing depositional environment, resulting in a high pyrite content. The interior of pyrite crystals is replete with organic matter, giving rise to pores within the organic matter during thermal evolution [Fig. 3(g)].

Inorganic pores in deep marine shale can be categorized into two groups: intragranular pores and intergranular pores. Intergranular pores develop between brittle minerals [Figs. 3(h) and 3(i)] and clay minerals [Figs. 3(j) and 3(k)]. These pores have different pore widths, and their shapes are mostly related to minerals. Most of the intragranular pores are dissolution pores, the pore diameters are less than 150 nm, and they are quadrilateral or circular. Unstable minerals close to organic matter are most likely to produce dissolution pores, mainly calcite and dolomite particles [Fig. 3(l)]. Therefore, intergranular pores in the Longmaxi Formation shale commonly occur between clay, pyrite, quartz, and other minerals. The diameters of these pores mostly range from tens of nanometers. The distribution of intragranular pores is dispersed, and there is a lack of connectivity between pore spaces.

The formation of microfractures is related to tectonic movement, hydrocarbon generation, montmorillonite dehydration, and other factors. Microfractures in deep shale are primarily dispersed within and along the peripheries of mineral particles. Shale is strongly influenced by tectonic activity, exhibiting evident occurrences of calcite-filled fractures [Fig. 4(a)]. Shale commonly exhibits tectonically induced fractures [Fig. 4(b)], with lengths reaching several tens of micrometers. These were occupied by clay minerals and carbonate minerals. Some microfractures are spread at the edges where organic matter and minerals contact, which is related to the shape of the mineral itself [Figs. 4(c) and 4(d)].

The formation of microfractures along the edges of organic matter may be related to dehydration shrinkage during the hydrocarbon generation process of organic matter. The microfractures within the brittle mineral and clay mineral interiors are generally straight, with no cement filling. These fractures have lengths ranging from 0.2 to 3  $\mu\text{m}$  [Figs. 4(e) and 4(f)].

### C. Quantitative characterization of pore structure

$\text{CO}_2$  adsorption has proven to be an efficacious technique for quantitatively delineating micropores in shale formations.<sup>49</sup> The maximum adsorption capacity of the deep marine shale samples varied from 0.73 to 3.19  $\text{cm}^3/\text{g}$ , with an average value of 1.81  $\text{cm}^3/\text{g}$  [Figs. 5(a)–5(c)]. The micropore volume, computed using the DFT model, falls within the range of 0.09–0.47  $\text{cm}^3/100\text{ g}$ , with an average of 0.24  $\text{cm}^3/100\text{ g}$ . Moreover, the micropore-specific surface area ranged from 5.08 to 23.78  $\text{m}^2/\text{g}$ , with an average of 13.78  $\text{m}^2/\text{g}$ . ORSS exhibited the most well-developed micropores, with an average micropore volume of 2.18  $\text{cm}^3/\text{g}$  and an average micropore-specific surface area of 16.53  $\text{m}^2/\text{g}$ . The pore width distribution curve exhibits two distinct peaks at 0.38–0.68 and 0.76–0.87 nm, indicating that the micropore volume is predominantly concentrated within these two intervals [Figs. 5(d)–5(f)]. The pore development degree of ORAS and ORMS is different. However, the distribution range of pore width is generally similar, which is the above two main development intervals.

$\text{N}_2$  adsorption experiments are employed for the quantitative characterization of mesopore structures in shale.<sup>50</sup> According to the categorization established by the International Union of Pure and Applied Chemistry (IUPAC), the hysteresis loop type of deep shale is mainly the  $\text{H}_2$  type, with a small amount of  $\text{H}_3$  type [Figs. 6(a)–6(c)]. This signifies that shale is predominantly distinguished by pores shaped like ink bottles, featuring narrow necks and broad bodies, with a limited quantity of pores resembling parallel plates. According to the pore width distribution curve, it is evident that the pore volume undergoes significant variations in the width range of 2–10 nm [Figs. 6(d)–6(f)]. According to the BJH model, the mesopore volume varies from 0.99 to 1.89  $\text{cm}^3/100\text{ g}$ , with an average of 1.53  $\text{cm}^3/100\text{ g}$ . According to the BET model, the mesopore-specific surface area spanned from 15.94 to 27.22  $\text{m}^2/\text{g}$ , demonstrating an average of 21.44  $\text{m}^2/\text{g}$ .

As delineated by the HPMT curves, upon reaching the displacement pressure, the mercury injection saturation rapidly increased. Subsequently, once the mercury injection saturation surpasses the 30% threshold, the increase in mercury injection gradually increases. The

TABLE I. Organic carbon content and mineral composition of shale samples (LZ stands for Luzhou area; CN stands for Changning area).

Sample ID	Depth (m)	TOC (%)	Mineral composition (%)							Lithofacies
			Quartz	Feldspar	Calcite	Dolomite	Pyrite	Clay	Other minerals	
LZ-1-1	3901.9	0.32	34	9	9	2	2	44	0	OPAS
LZ-1-2	3949.0	0.67	29	7	11	5	2	46	0	OPAS
LZ-1-3	4013.5	2.33	43	6	3	4	4	40	0	ORAS
LZ-1-4	4019.2	2.37	37	6	4	4	5	44	0	ORAS
LZ-1-5	4021.4	3.14	27	8	5	31	2	27	0	ORMS
LZ-1-6	4025.0	4.74	44	7	5	5	2	37	0	ORSS
LZ-1-7	4029.3	4.09	39	10	4	2	5	40	0	ORAS
LZ-1-8	4032.5	3.90	33	5	11	15	4	32	0	ORMS
LZ-1-9	4032.8	3.95	44	10	9	7	4	26	0	ORSS
LZ-1-10	4037.1	0.07	54	4	3	6	6	27	0	OPSS
LZ-2-1	4004.5	2.61	37	7	6	6	3	41	0	ORAS
LZ-2-2	4021.2	3.25	46	5	3	10	3	33	0	ORSS
LZ-2-3	4031.2	4.28	56	4	2	10	4	24	0	ORSS
LZ-2-4	4034.5	4.22	31	6	3	24	3	33	0	ORMS
LZ-2-5	4035.2	4.43	41	4	15	17	5	18	0	ORMS
LZ-2-6	4039.3	3.94	55	4	7	16	3	15	0	ORSS
LZ-2-7	4042.7	3.15	46	4	11	22	2	15	0	ORMS
CN-1-1	4297.3	1.74	30	22	35	1	3	10	0	OFMS
CN-1-2	4301.7	1.74	31	0	11	16	5	36	2	OFMS
CN-1-3	4302.1	3.48	36	12	4	0	4	43	2	ORAS
CN-1-4	4307.2	3.90	42	9	7	0	8	35	0	ORSS
CN-1-5	4310.4	3.90	34	0	10	16	7	30	3	ORMS
CN-1-6	4316.1	3.86	56	7	9	5	6	16	1	ORSS
CN-1-7	4321.8	6.93	44	7	17	13	4	14	1	ORMS
CN-1-8	4327.4	3.24	62	7	7	5	5	14	1	ORSS
CN-2-1	3884.6	2.95	43	7	19	11	1	19	0	ORMS
CN-2-2	3918.0	1.34	32	2	11	13	6	33	2	OFMS
CN-2-3	3939.5	2.35	34	5	8	18	0	35	2	ORMS
LZ-3-1	4116.1	2.41	53	5	10	5	6	20	1	ORSS
LZ-3-2	4119.7	2.98	71	2	10	5	3	9	1	ORSS
LZ-3-3	4121.5	3.12	70	4	7	7	3	9	0	ORSS
LZ-3-4	4092.5	2.53	27	11	4	5	0	51	2	ORAS
LZ-3-5	4118.4	2.91	45	4	4	3	0	41	3	ORAS
LZ-3-6	4135.2	4.05	58	5	3	3	0	28	3	ORSS
LZ-3-7	4140.9	4.76	39	6	5	6	0	32	12	ORSS
LZ-3-8	414.2	2.75	39	3	11	34	0	11	2	ORMS

maximum mercury saturation of the shale varies from 60.9% to 94.7%, with an average of 82.4% [Figs. 7(a)–7(c)]. This indicates that the increase in pore volume diminishes as the pore width expands. When the pore diameter is less than 100 nm, the curve changes significantly, indicating that pores with diameters less than 100 nm substantially contribute to the overall pore volume [Figs. 7(d)–7(f)]. According to the parameters of the pore structure, the mean pore width varies between 61 and 160 nm, with an average measurement of 126 nm. The volume of the pores ranges from 0.58 to 1.54 cm<sup>3</sup>/100 g, with an average of 0.97 cm<sup>3</sup>/100 g. The surface area specific to the pores ranges from 1.31 to 3.46 m<sup>2</sup>/g, with an average value of 2.16 m<sup>2</sup>/g.

V. DISCUSSION

A. Controlling factors of deep marine pore development characteristics

1. Pore structure

A correlation analysis was performed to explore the relationships between the multiscale pore structure parameters and both the TOC content and mineral composition. The findings reveal variations in the governing factors of pore structure across diverse lithofacies. Within a certain range of ORMS and ORAS samples (TOC < 4%), the evolution of micropores, mesopores, and the specific surface area exhibited a

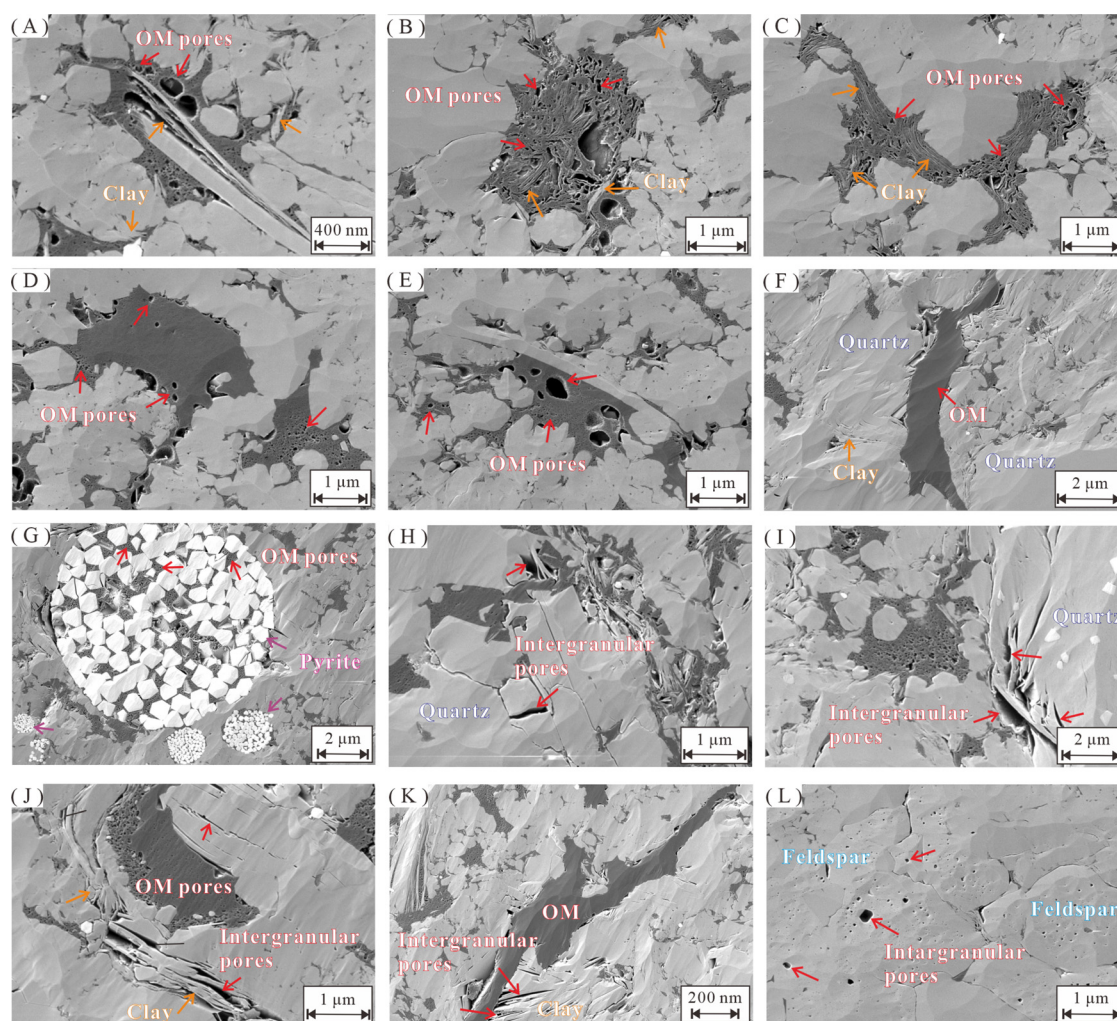


**FIG. 3.** Photographs showing the OM pore features of samples. (a) The organic matter filled in the chlorite bedding develops a large number of elliptical and point-shaped organic pores. (b) and (c) Organic matter filled between mineral particles, associated with clay minerals, a large number of elliptical OM pores are developed and distributed in strips. (d) Partially dense needlelike pores in organic matter. (e) OM pores scales are significantly different and heterogeneous. (f) Strip-shaped organic matter does not develop its pores, but develops slit-like pores at the edge of contact with mineral particles. (g) The organic matter filled between strawberry-like pyrite grains develops a large number of irregular OM pores. (h) and (i) Intergranular pores between quartz grains, pore width is large and the distribution is scattered, and the pores are not connected. (j) and (k) Clay minerals exhibit numerous intergranular pores, featuring diameters in the tens of nanometers and exhibiting robust connectivity. (l) Angular intragranular dissolution pores emerge on the surface of feldspar minerals.

definite positive correlation with the TOC content [Figs. 8(a), 8(c), 8(f), and 8(h)]. The impact of the clay mineral content on pore development is especially evident in ORMS and displays a favorable correlation with the progression of micropores, mesopores, and specific surface area [Figs. 8(b), 8(d), 8(g), and 8(i)]. In the ORSS specimens, given the elevated TOC content, the extent of pore advancement exhibited a subdued connection with the organic matter content. Nonetheless, there exists a specific positive correlation between the quartz content and the progression of pore development [Fig. 8(e)]. A definite positive correlation is observed between quartz and TOC in the research region, signifying that the origin of silica was primarily biogenic. Therefore, there is a correlation between the siliceous mineral content and TOC content. In addition, siliceous minerals have good

pressure resistance and play a role in protecting pores during diagenesis. Due to the brittleness of siliceous minerals, cracks are generated during the later fracturing process to improve the physical properties of the reservoir.

Previous studies have demonstrated that different clay minerals exhibit distinct pore structures, and significant variations are observed in their specific surface areas.<sup>51–53</sup> Clay minerals generate a multitude of pores, with montmorillonite clay exhibiting the most developed micropores, followed by illite/smectite minerals. ORSS encompasses a lower quantity of clay minerals, and its clay composition predominantly comprises illite, with only a minor presence of an illite/montmorillonite mixed layer. Consequently, clay minerals contribute minimal pores and exert limited influence on the overall porosity of



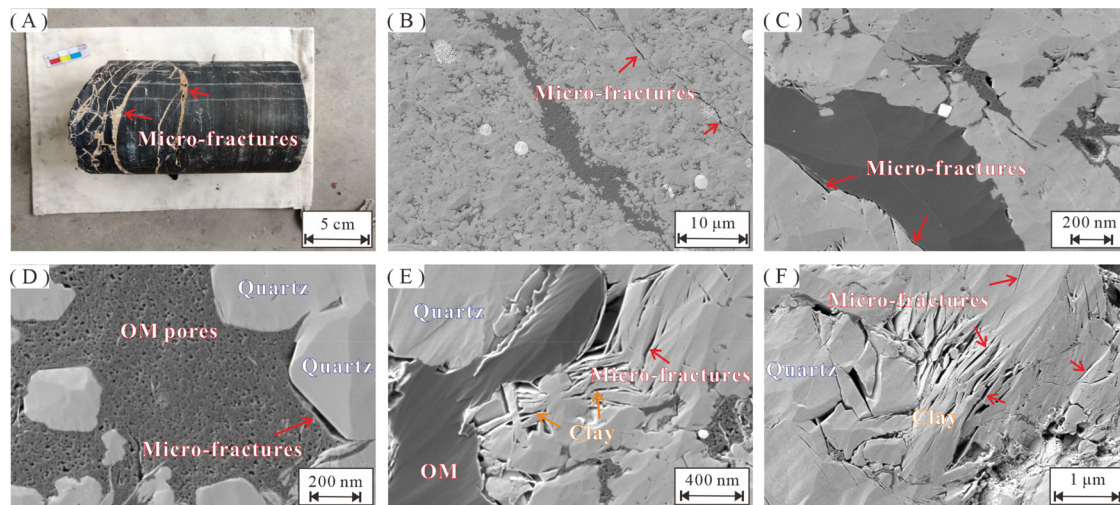


**FIG. 4.** Photographs showing the micro-fracture features of samples. (a) Calcite veins filling micro-fractures. (b) Micro-fractures of tectonic origin, up to tens of micrometers in length, filled with calcite mineral. (c) and (d) Micro-fractures emerge at the boundary between organic matter and inorganic minerals. (e) and (f) Micro-fractures develop inside brittle mineral and clay mineral particles and are not filled.

the shale. Additionally, the dissolution of soluble minerals through organic acids generated during hydrocarbon production further stimulates the creation of secondary pores.<sup>54–56</sup> In the case of ORMS and ORAS, the configuration of pores is governed by the interplay between TOC and clay minerals. The proportion of organic matter is modest, thereby restricting the growth of OM pores. Conversely, elevated levels of clay minerals can engender a significant quantity of pores, including interlayer pores, intercrystalline pores, and contraction joints formed through dehydration. Organic matter is commonly linked with clay minerals. Throughout the diagenesis process, the conversion of

montmorillonite to illite can decrease the activation energy of thermal decomposition reactions. This catalytic effect on the pyrolysis of kerogen enhances the rate of thermal decomposition and promotes the development of OM pores.

## 2. Fractal dimension

Previous studies have indicated distinct heterogeneity in shale pore structure. The fractal dimension provides a quantitative means to characterize the intricacy and diversity of irregularities within a pore

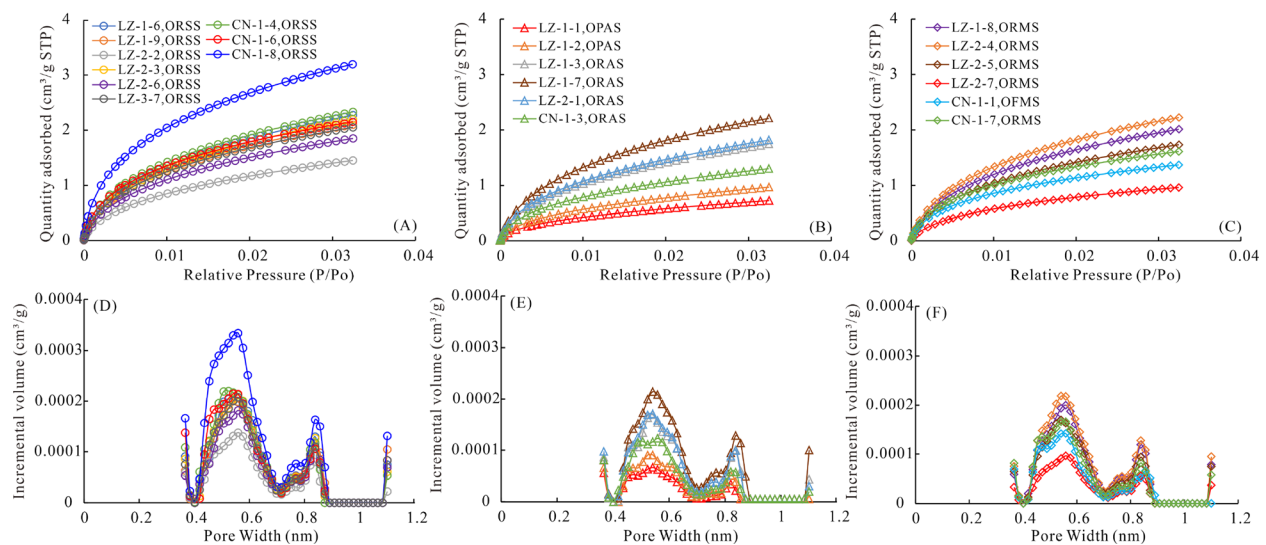


**FIG. 5.** Pore structure characteristics based on the CO<sub>2</sub> adsorption method. (a) CO<sub>2</sub> adsorption isotherms of ORSS. (b) CO<sub>2</sub> adsorption isotherms of ORAS. (c) CO<sub>2</sub> adsorption isotherms of ORMS. (d) Pore width distribution of ORSS from CO<sub>2</sub> adsorption. (e) Pore width distribution of ORAS from CO<sub>2</sub> adsorption. (f) Pore width distribution of ORMS from CO<sub>2</sub> adsorption.

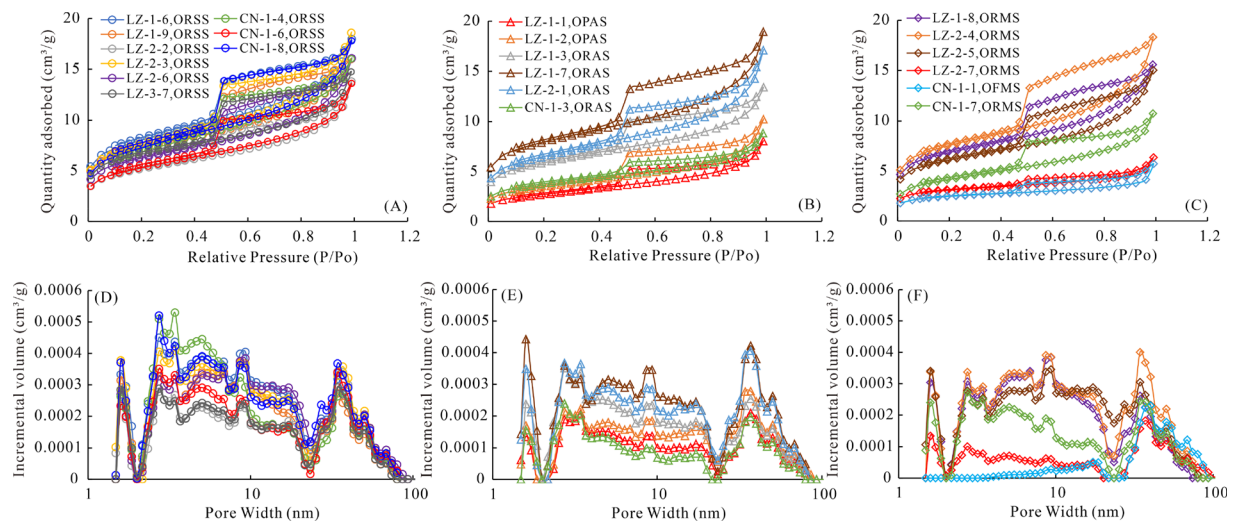


**FIG. 6.** Pore structure characteristics based on the N<sub>2</sub> adsorption method. (a) N<sub>2</sub> adsorption-desorption isotherms of ORSS. (b) N<sub>2</sub> adsorption-desorption isotherms of ORAS. (c) N<sub>2</sub> adsorption-desorption isotherms of ORMS. (d) Pore width distribution of ORSS from N<sub>2</sub> adsorption. (e) Pore width distribution of ORAS from N<sub>2</sub> adsorption. (f) Pore width distribution of ORMS from N<sub>2</sub> adsorption.

structure.<sup>8,57–59</sup> In this study, the FHH model was employed to compute the fractal dimension for characterizing the pore structure. A fractal dimension nearing 2 suggests a comparatively uniform pore structure, while a fractal dimension nearing 3 signifies elevated complexity in the pore structure. According to the DFT equation, a relative pressure ( $p/p_0$ ) of 0.45 corresponds to a pore diameter of 4.34 nm. Hence, the domain where  $p/p_0 < 0.45$  can be categorized as a low-pressure zone, indicating pores with diameters less than 4.34 nm. Conversely, the realm where  $p/p_0 > 0.45$  is designated a high-pressure zone, denoting relatively substantial pores with diameters ranging

from 4.34 to 100 nm. In the computation of the fractal dimension, the adsorption isotherms in the low-pressure and high-pressure zones are individually fitted and computed. This yields two distinct fractal dimensions:  $D_1$  for small pores and  $D_2$  for larger pores. In SEM, the attributes of shale pore structures indicate that the morphology of OM pores undergoes a shift from intricate reticular patterns to comparatively simpler formations, such as sponge-like structures, as the pore width decreases. With further reduction in pore size, the configuration of organic matter pores is expected to become more straightforward. This occurrence explains why the fractal dimension  $D_2$  surpasses  $D_1$ .

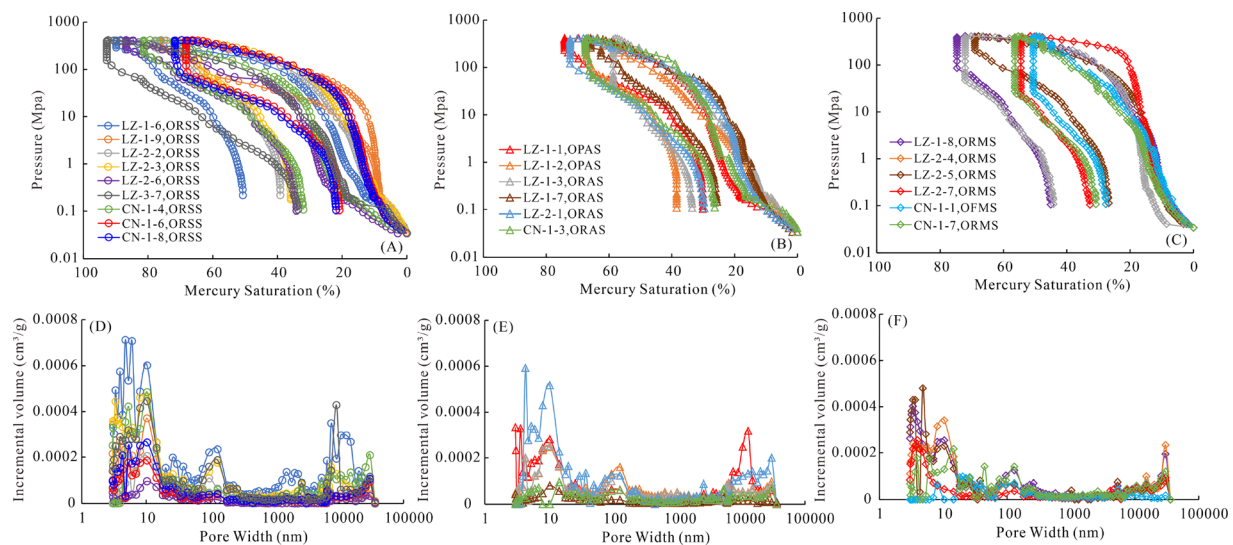


**FIG. 7.** Pore structure characteristics based on the HPMI method. (a) Mercury intrusion and extrusion curves of ORSS. (b) Mercury intrusion and extrusion curves of ORAS. (c) Mercury intrusion and extrusion curves of ORMS. (d) Pore width distribution of ORSS from HPMI. (e) Pore width distribution of ORAS from HPMI. (f) Pore width distribution of ORMS from HPMI.



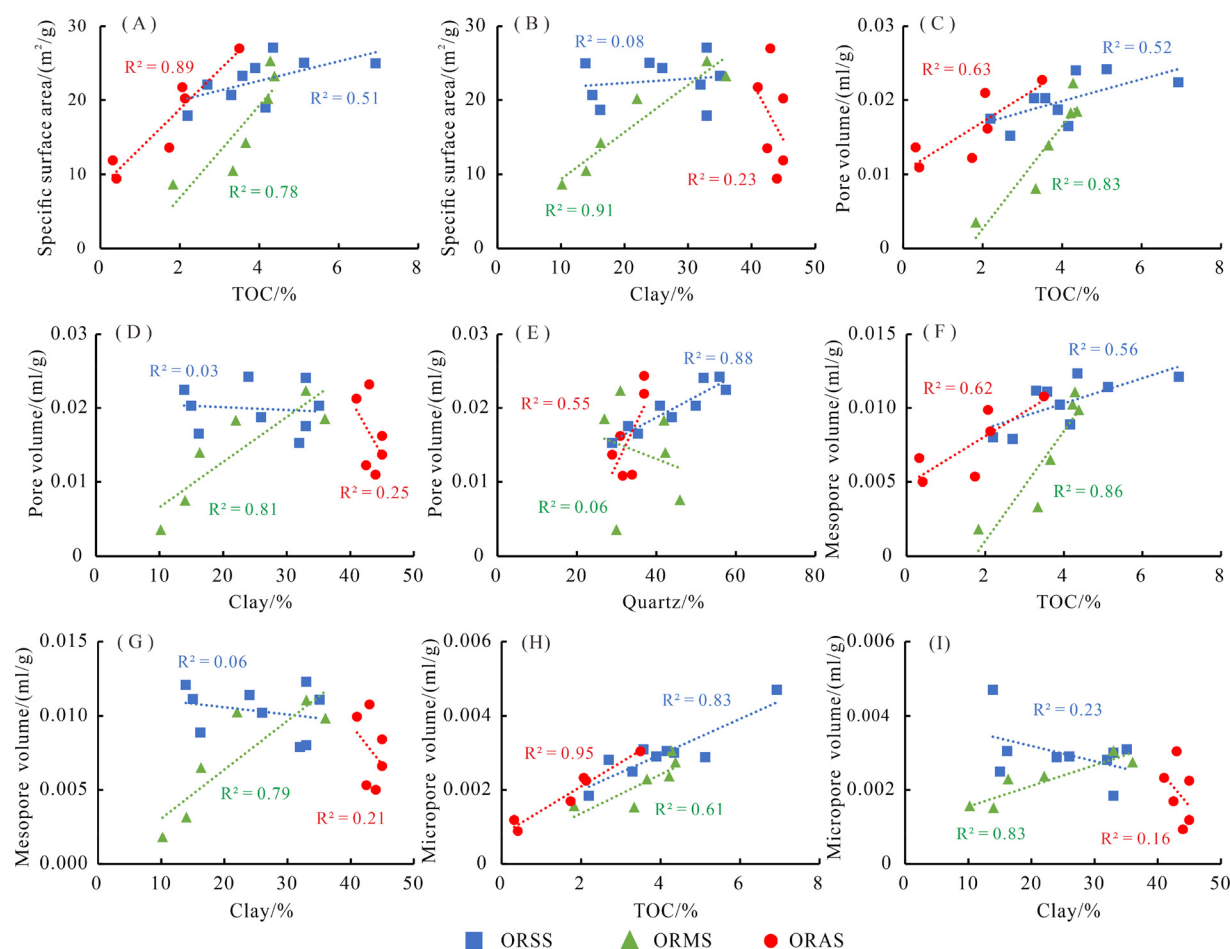


**FIG. 8.** Scatter charts of correlations between pore structure and shale composition. (a), (c), (f), and (h) Correlation between the pore structure of distinct lithofacies and TOC. (b), (d), (g), and (i) Correlation between the pore structure of distinct lithofacies and clay. (e) Correlation between the pore structure of distinct lithofacies and quartz.

For ORSS, the substantial advancement of OM pores results in an increase in micropore volume, a decrease in mean pore size, and a decrease in micropore intricacy. Conversely, larger pores become more intricate due to the proliferation of micropores, as indicated by a decrease in  $D_1$  and an increase in  $D_2$  [Figs. 9(a), 9(d), 9(i), and 9(l)]. The pores formed by minerals such as quartz are mainly concentrated in the mesopore to macropore range. An increase in quartz content increases the number of larger pores, thereby increasing the complexity of these larger pores while reducing the complexity of smaller pores. This is manifested by an increase in the value of  $D_2$  and a decrease in the value of  $D_1$  [Figs. 9(c), 9(f), 9(h), and 9(k)]. Moreover, a favorable correlation exists between quartz and organic matter. The increase in quartz minerals reflects the increase in organic matter micropores, which in turn leads to a decrease in the value of  $D_1$ . On the other hand, under excessive thermal maturation, clay minerals can only provide a limited number of pores. An increase in the clay mineral content partially stimulates the progression of micropores, augmenting the intricacy of smaller pores primarily governed by OM pores [Fig. 9(b)].

In the case of ORMS and ORAS, as the concentration of clay minerals increases, there is a concurrent increase in the quantity of

smaller pores, encompassing micropores, and certain mesopores, leading to an increase in the complexity of the shale pore surface and structure. Consequently, the fractal dimension  $D_1$  experiences a corresponding increase [Figs. 9(b), 9(e), 9(i), and 9(l)]. An increase in the TOC content signifies a heightened prevalence of smaller pores in shale, thereby amplifying the intricacy of the small pore system. This, in turn, leads to an increase in the fractal dimension  $D_1$  [Figs. 9(a), 9(i), and 9(l)]. Compared to the features observed in ORSS, the increase in quartz content contributes to the existence of more substantial pores, resulting in an increase in the fractal dimension  $D_2$  and a decrease in the  $D_1$  [Figs. 9(b) and 9(e)].

## B. Genesis mechanisms of high-quality reservoirs in deep shale formations

The deep marine shale reservoir exhibits a coupled characteristic of high biogenic silica, high organic carbon, and abundant organic matter pores. The hydrocarbon-generating organisms in the Longmaxi Formation shale are predominantly multicellular algae, with single-celled algae as a secondary component.<sup>60,61</sup> Multicellular algae possess

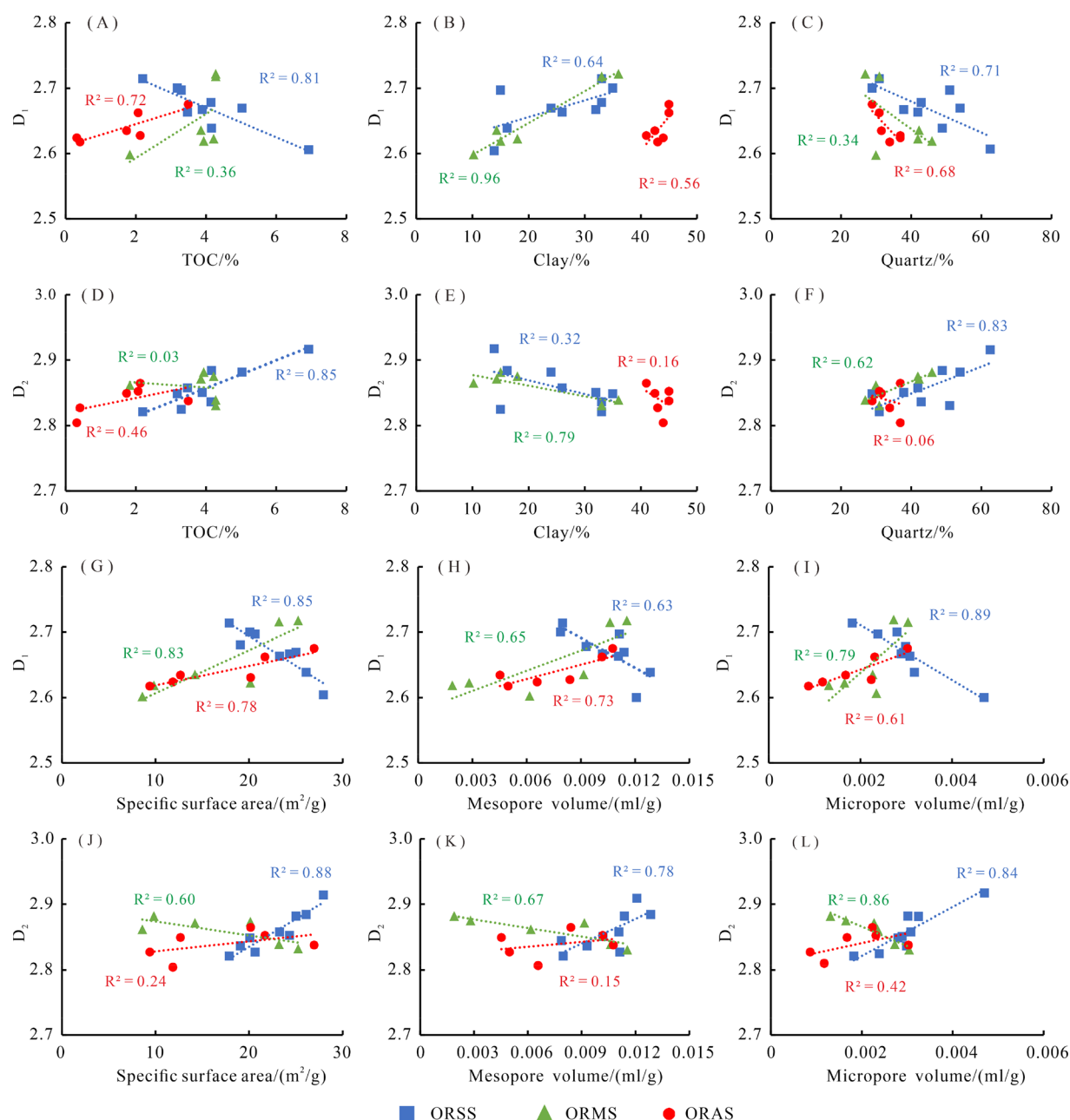


**FIG. 9.** Scatter charts of between Fractal dimension and shale composition and pore structure. (a) and (d) Correlation between the fractal dimension of distinct lithofacies and TOC. (b) and (e) Correlation between the fractal dimension of distinct lithofacies and clay. (d) and (f) correlation between the fractal dimension of distinct lithofacies and quartz. (g) and (i) Correlation between the fractal dimension of distinct lithofacies and specific surface area. (h) and (k) Correlation between the fractal dimension of distinct lithofacies and mesopore volume. (i) and (l) Correlation between the fractal dimension of distinct lithofacies and micropore volume.

a strong hydrocarbon generation capacity and the ability to create organic pores. The abundance of multicellular algae contributes to the high TOC of this shale section. This leads to the formation of more organic pores and a three-dimensional interconnected pore network, which facilitates the occurrence and production of shale gas.

Based on the geological conditions and experimental analysis of shale gas formation, this study investigates the mechanisms of shale hydrocarbon generation and storage from petrology, mineralogy, geochemistry and other perspectives. It is observed that the biogenic silica in the deep-water shelf facies undergoes continuous dehydration and gradually transforms into rigid crystalline quartz during diagenesis.<sup>62</sup>

A large number of quartz particles form a relatively rigid framework. Concurrently, micron-sized intergranular pores are generated between the quartz particles, providing storage space for early retained oil. As thermal evolution progresses and burial deepens, liquid hydrocarbons within the reservoir and intergranular pores undergo cracking. This leads to the generation of large amounts of natural gas, while the formation of organic pores enhances the compaction resistance of quartz intergranular pores, thereby protecting a significant number of primary and diagenetic secondary pores. Therefore, the biogenic silica in the Longmaxi Formation not only helps preserve primary intergranular pores in shale prior to hydrocarbon charging but also facilitates the later preservation of organic pores formed during hydrocarbon cracking. In conclusion, biogenic silica offers the advantage of resisting compaction, thereby preserving pore spaces, which is fundamental to pore development.

Structural conditions play an important role in the development of high-quality shale reservoirs. In southern Sichuan, the deep structural conditions are complex, with low-angle and gentle structures, as well as faults. Except near faults, the reservoir pressure in different structural regions is relatively high, with pressure coefficients reaching approximately 1.7–2.0 (Fig. 10). The high production rates of high pressure gas wells in shale indicate that the elevated pressure in deep layers plays a protective role in preserving the pores of shale reservoirs. High reservoir pressure promotes intra-pore support, which, in combination with high-strength siliceous minerals (primarily quartz), forms a rigid skeletal framework. In a closed diagenetic environment, organic acids continuously dissolve calcareous minerals, ensuring that the porosity of shale reservoirs remains largely unchanged as burial depth increases. Furthermore, structural deformation leads to the development of various types of fractures, such as lateral extension and inter-layer slip, in deep synclinal areas. The fracture density increases toward the core, effectively enhancing the connectivity between

reservoir pores and fractures, thereby improving the reservoir's storage capacity and the high production potential of gas wells.

## C. Transport mechanism and characteristics of deep marine shale gas

### 1. Classification of gas transport mode

Fractal dimension can characterize the complexity of pore space, which is used to establish the relationship between pore structure and natural gas transport mode. The differences in fractal characteristics at multiscale pores can serve as one of the fundamental criteria for classifying shale pore systems. The size and morphology of pores directly influence the incidence and transportation methods of gas. The gas transport mode in porous media combined with the Knudsen number (Kn) is used to characterize the microscopic transport mechanism of gas in shale.<sup>25,63–66</sup> Based on experimental testing and fractal model results, the fractal characteristics of pores during the low-pressure stage (pore width larger than 4.34 nm) are significantly pronounced. This indicates that flow-diffusion pores with relatively larger pore widths exhibit distinct fractal features. The pore system of deep shale is divided into three categories: ultramicro adsorption pores (<1.20 nm), nano-diffusion pores (1.20–4.34 nm), and micro/nano flow-diffusion pores (>4.34 nm) (Fig. 10). Ultramicro adsorption pores are mainly sponge-like OM pores. Nano-diffusion pores are mainly OM pores and clay mineral pores. Micro/nano flow-diffusion pores are mainly inorganic pores and micrometer-scale bubble-like OM pores and microfractures.

Gas transport mechanisms can be further categorized as follows. Within the range of ultramicro adsorption pores (<1.2 nm), the transport mode for methane molecules is surface adsorption-diffusion. The mechanism underlying surface adsorption-diffusion involves the jumping process of gas molecules on the solid surface. In organic matter with a substantial specific surface area, surface adsorption-diffusion plays a crucial role as an important transport mechanism. Within the range of nano diffusion pores (1.2–4.34 nm), the predominant gas transport mode is Knudsen diffusion ( $1 < Kn < 10$ ), which represents a transitional transport mechanism combining adsorption and diffusion. Within the range of micro-nano flow-diffusion pores (>4.34 nm), the gas transport modes can be further classified into Fick diffusion (4.34–15.00 nm), slip flow (15–180 nm), and continuous flow (>180 nm). Therefore, the deep marine pore system is classified into three major categories, each corresponding to five different gas transport modes (Fig. 11). This classification facilitates the establishment of the link between gas transport mode and pore characteristics.

### 2. Controlling effect of pore structure on gas transport

The evolution features of pore structure, encompassing the distribution of pores, morphology, and spatial arrangement, are immediate factors influencing the mode of gas transport.<sup>11,67–70</sup> In shale, the interplay among gas molecules and the interactions between molecules and pore walls play pivotal roles in directly shaping gas transport. This is manifested by controlling the efficiency of gas transport within the shale. For instance, in cases where the pore width is diminutive (considerably smaller than the average free path of gas molecules), the likelihood of collisions between gas molecules and the pore wall surpasses the likelihood of collisions among gas molecules themselves. As a

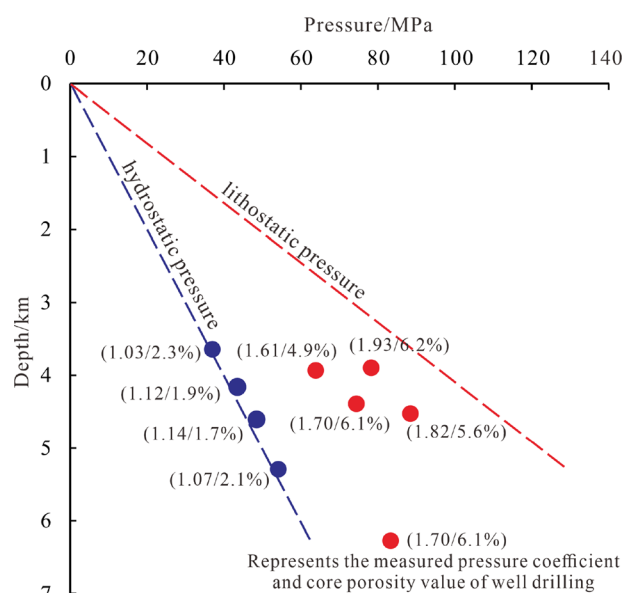


FIG. 10. Porosity characteristics of Longmaxi shale in southern Sichuan basin under different formation pressure.

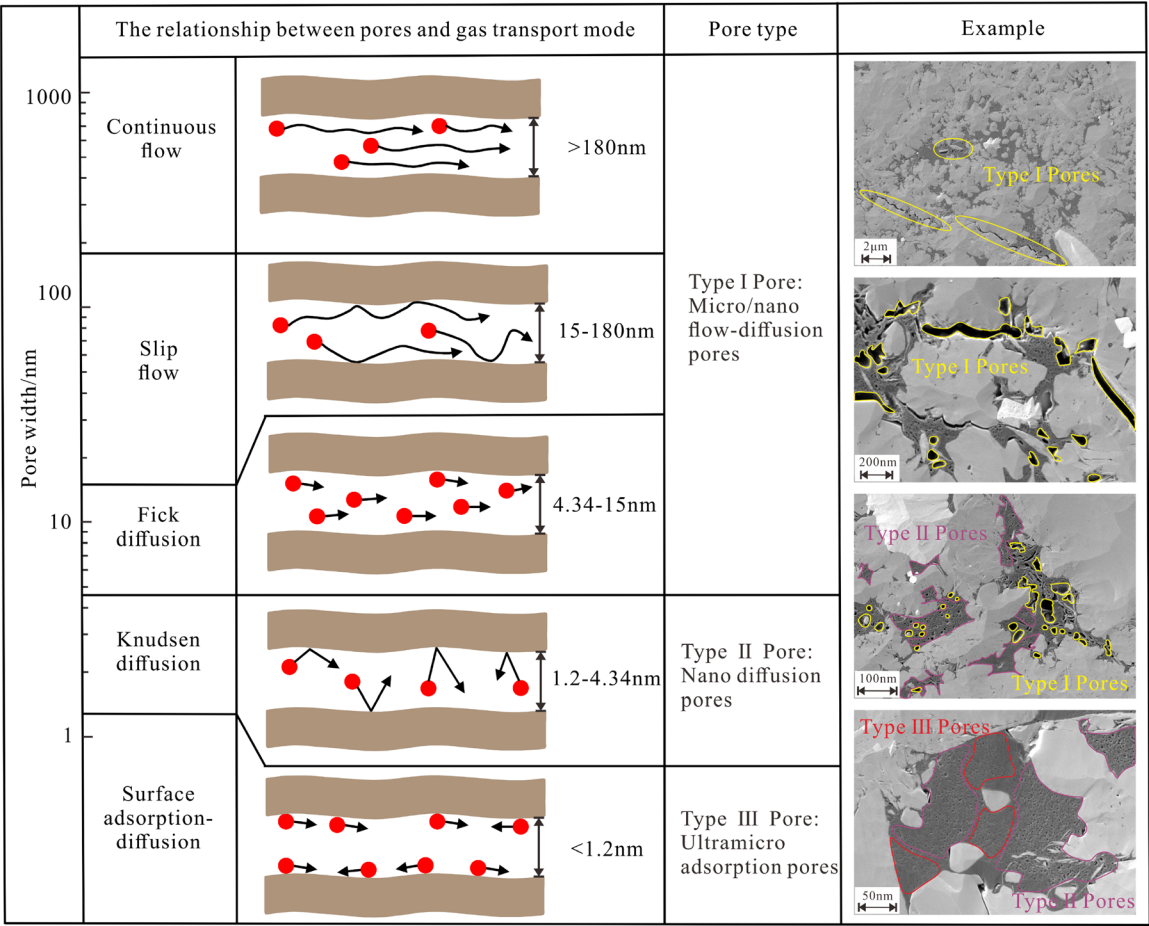


FIG. 11. The division scheme of five gas transport modes in deep shale and the corresponding pore classification.

result, the hindrance to gas transport through microchannels is predominantly determined by the interactions between gas molecules and the pore wall.

In the ORSS and ORMS reservoirs, surface adsorption-diffusion pores are present [Figs. 12(a)–12(d)], with a significant proportion occupied by OM pores. The surface adsorption-diffusion pores that develop in reservoirs tend to be fine and isolated. Slip flow pores, characterized by high openness and relatively good connectivity, exhibit a certain degree of development. However, the development of continuous flow pores is relatively low, and these pores are relatively isolated. The pore development in ORAS occurs between continuously flowing pores and surface adsorption-diffusion pores [Figs. 12(e) and 12(f)], which possess the capacity to host nanoscale pores and a certain degree of slip flow release capability. In summary, deep shale lacks continuous flow pores, resulting in large-scale adsorption storage spaces that are relatively independent and lack gas transmission paths. The deep shale in southern Sichuan exhibits a strong adsorption capacity and is characterized by relatively low natural permeability.

The permeability test of shale only represents the overall permeability of shale. The ability of gas to transport outward from different types of nanopore spaces needs to be studied more

accurately. In shale composed of nanoscale pores, slip flow, and diffusion are the dominant gas transport mechanisms. The overall permeability of deep shale is affected by the characteristics of microfractures. In the shale matrix separated by fractures, gas transport is controlled by a multilevel flow field consisting of adsorption-diffusion pores and microfractures. Utilizing the categorization of pore systems and the modes of gas transport, the deep marine shale flow fields are categorized into surface adsorption-diffusion, Knudsen diffusion, Fick diffusion, slip flow, and continuous flow (Fig. 13). The permeability of the pore system is determined by the slowest flow mechanism among these flow fields.

Deep shale formations typically exhibit a favorable capacity for methane accumulation. In particular, the presence of well-developed adsorption-diffusion pores with strong adsorption and storage capabilities contributes significantly to this methane accumulation. Within the pore framework of profound shale reservoirs, OM pores are predominantly developed at the nanoscale. However, there is a lack of connectivity between these nanoscale pores and the space for continuous flow (Fig. 13). The lack of development of continuous flow space limits the production process of deep marine shale formations with low permeability and difficult development.

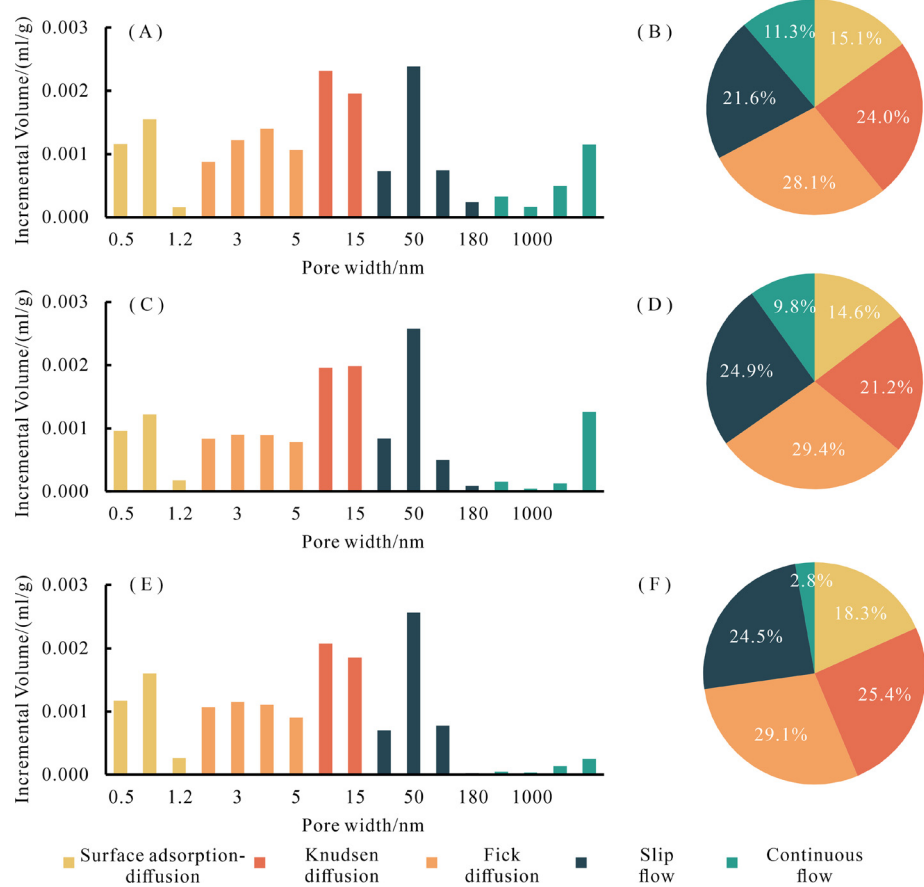


FIG. 12. Statistical diagram of pore diameters in different lithofacies gas transport modes. (a) and (b) illustrate the distribution of pore and the proportion of various gas transport modes in ORSS. (c) and (d) illustrate the distribution of pore and the proportion of various gas transport modes in ORMS. (e) and (f) illustrate the distribution of pore and the proportion of various gas transport modes in ORAS.

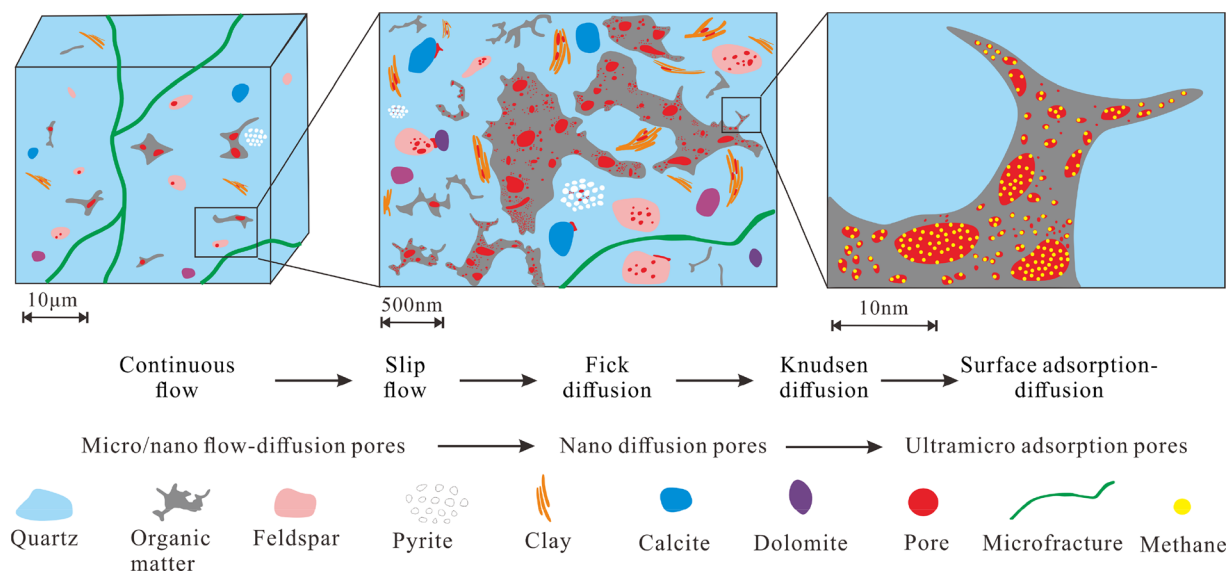


FIG. 13. Schematic diagram of the effect of multi-scale pore structure on gas transport mode in deep shale.



#### D. Differences in pore structure between deep and shallow marine shale

There is no obvious difference between deep and shallow shales in terms of the intrinsic factors of the shale pore structure, such as the TOC content and mineral composition. Due to variations in burial depth, external factors such as pressure and temperature assume a pivotal function in the feature of pore structures.<sup>71–73</sup> Based on the shale porosity data from static tests, deep shale reservoirs still exhibit relatively high porosity. The porosities of the deep and shallow shales are generally comparable, with the main distribution falling within the range of 3%–6% (Fig. 14). Further analysis is required to reveal the significant differences in pore types and characteristics between deep and shallow shale layers, which constitute important factors influencing variations in shale gas development yields.

The N<sub>2</sub> adsorption-desorption isotherms of shale samples at shallower depths in the outskirts of the Sichuan Basin display a hysteresis loop characterized by a blend of H<sub>2</sub> and H<sub>3</sub> types,<sup>72–75</sup> demonstrating the presence of both slit-like pores and bottle-necked pores. In contrast, the deep shale samples display a predominantly H<sub>2</sub>-type morphology, indicating the predominant development of bottle-necked pores. This is attributed to the influence of their own structure under deep burial conditions, where slit-like pores, with internal fluids extruded under compression, become more susceptible to compaction effects. Consequently, this portion of the pores rapidly decreases. In contrast, bottle-necked pores exhibit poor connectivity, allowing them to better maintain pore pressure and resist the influence of compaction.

A quantitative examination of the distribution of diverse pore categories in deep and surface-level shale revealed that micropores and mesopores are more extensively evolved in deep shale than in shallower shale.<sup>76</sup> In deep shale, micropores and mesopores predominantly

consist of OM pores, dissolution pores, and clay mineral pores [Fig. 15(a)]. Conversely, OM pores dominate the micropores and mesopores of the shallow shale [Fig. 15(b)]. This suggests that under deep burial conditions, mesopores in shale samples undergo significant compaction, compression, and evolution into smaller micropores. Additionally, the high pressure coefficient in deep gas reservoirs and overpressure play a role in preserving small pores. Consequently, mesopores transform into a larger volume of micropores. The macropores in shallow shale are more developed than those in deep shale, primarily consisting of microfractures and interstitial pores between inorganic minerals. Shallow shale, influenced by later tectonic movements leading to stratigraphic uplift and reduced pressure, experiences the development and preservation of microfractures. In contrast, there are fewer developed microfractures in the deep shale layers than in the shallow layers.

Distinctive changes in physical properties under different burial depths and overburden pressure conditions reveal an exceptionally strong stress sensitivity in fractured reservoirs of shallow shale. In comparison to matrix porosity, the pore volume of fractured-type reservoirs under a 35 MPa overburden pressure has decreased to approximately 38% of the initial pore volume [Fig. 16(a)]. The pressure sensitivity of matrix porosity is significantly weaker than that of fractured-type reservoirs, with pore volume generally maintained at over 80% of the initial porosity under pressure conditions ranging from 35 to 50 MPa. Siliceous shale exhibits a slightly greater degree of pore volume retention than argillaceous shale [Fig. 16(a)]. In the Jiaoshiban area, the effective stress of the Longmaxi Formation is approximately 30 MPa. Under geological conditions, microfractures may occupy a low proportion of the reservoir space, but their impact

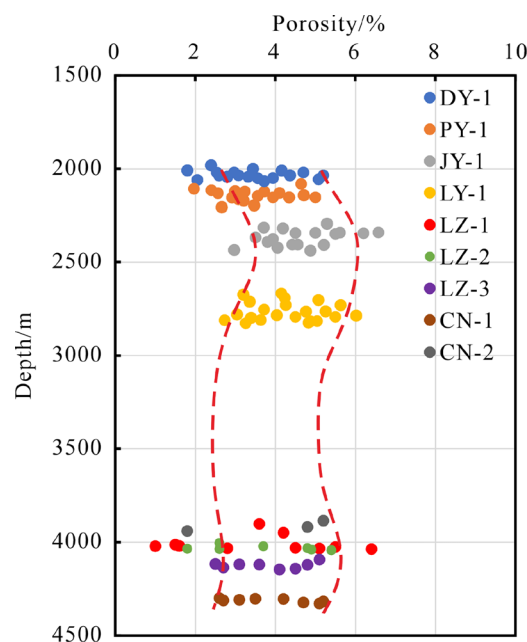


FIG. 14. Characteristics of porosity in deep and shallow marine shale.

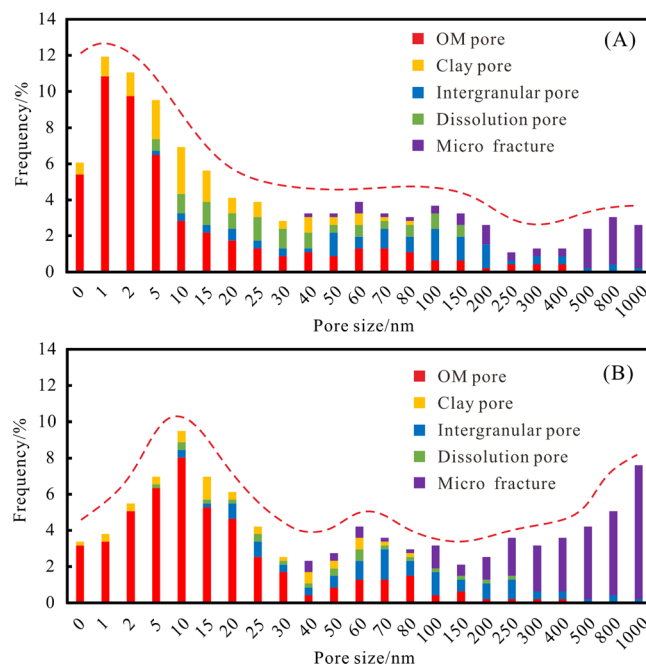
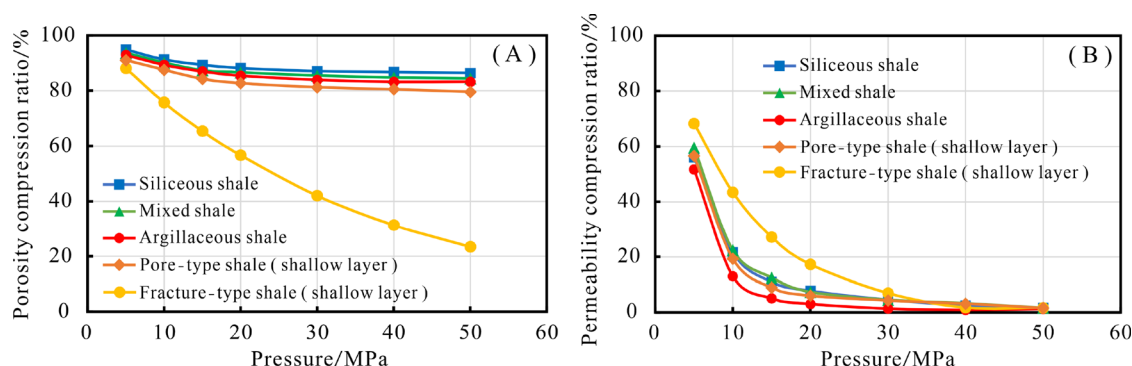


FIG. 15. The pore width distribution characteristics of different types of pores in deep and shallow marine shale: (a) deep marine shale (Luzhou area sample) and (b) shallow marine shale (Jiaoshiba area sample).



**FIG. 16.** The characteristics of porosity and permeability variations with pressure in different shales: (a) characteristics of porosity variation with pressure and (b) characteristics of permeability variation with pressure. Note: Siliceous shale sample is CN-1-8, Mixed shale sample is LZ-1-8, Argillaceous shale sample is LZ-1-7, and Pore-type shale sample and fracture-type are longmaxi Formation shale of jiaoshiba area.

on permeability can be substantial. Both fracture permeability and matrix porosity permeability exhibit strong pressure sensitivity, with permeability sharply decreasing with increasing pressure. At 30 MPa, the permeability decreased to less than 10% of the initial permeability [Fig. 16(b)]. By comparison, the matrix porosity rapidly decreases to below 20% before the pressure reaches 10 MPa [Fig. 16(b)]. As the pressure continues to increase, the rate of decrease becomes noticeably slower, with siliceous shale exhibiting a slightly lower rate of decline than argillaceous shale. For the fracture permeability, the rate of decrease is lower than that for the matrix porosity permeability before reaching 30 MPa. Fracture permeability generally surpasses matrix porosity permeability (possibly related to subtle slip in microfractures). At 35 MPa, the compression ratios of the fracture permeability and matrix porosity permeability are similar, and the contribution of fractures to the permeability tends to decrease. The 35 MPa pressure is equivalent to the depth near 3500 m, precisely corresponding to the depth boundary between deep and shallow shale gas reservoirs. Therefore, although microfractures contribute less to reservoir porosity, their contribution to the permeability of shallow shale gas is crucial. Under deep conditions, fracture permeability is comparable to matrix porosity permeability, leading to a significant decrease in the contribution of fractures to shale permeability. This is also a crucial reason why effective enhancement and stable high production are challenging in deep shale.

### E. Guidance for deep shale gas exploration and development

The Sichuan Basin experienced stable subsidence before the Early Triassic, uplift during the Late Triassic to Early Cretaceous, and uplift during the Himalayan period. These multistage tectonic shifts have exerted a substantial influence on the shale gas reservoir of the Silurian Longmaxi Formation.<sup>76,77</sup> These tectonic events exerted a substantial influence on the Paleozoic marine strata, resulting in a more fragmented and disrupted structural setting. Multiple phases of widespread uplift caused the tectonic stabilization phase in the southern Sichuan area to occur long after the hydrocarbon generation and accumulation phase.<sup>78</sup> As a consequence, the free-state gas in the region faces extremely unfavorable conditions for accumulation. The conventional approach of focusing on structural traps such as anticlines and fault

sealing has encountered challenges in deep shale gas exploration in the southern Sichuan area. Further research is required to explore the possibilities of micro/nanoscale pore-fracture networks and the potential for primary source-to-reservoir adsorption accumulation. In such cases, the trapping mechanism for hydrocarbons shifts from buoyancy to reservoir pressure, which is essentially the pressure exerted by the pore fluids within the rock formation. The Longmaxi Formation shale in the southern region of Sichuan exhibits elevated silica content and is characterized by a pore system predominantly governed by OM pores. These attributes offer advantageous storage capacity and preservation conditions conducive to the adsorption and free gas of deep marine shale. The shale within the Longmaxi Formation is abundant in organic matter, featuring a moderate level of thermal maturity. This establishes a robust groundwork for the generation of shale gas. In the area with weak tectonic deformation, the shale gas of Longmaxi Formation is well preserved and has good potential for resource exploration.

According to the findings of the research, the  $D_1$  parameter of ORSS exhibits a converse correlation with the specific surface area and volume of pores. This indicates that an escalation in the  $D_1$  value corresponds to a reduction in the shale's capacity for storing free gas. However,  $D_1$  values are influenced by mineral composition. The low  $D_1$  value is related to the increase in brittle mineral and the decrease in clay mineral, which is beneficial to the fracturing mining process. The  $D_2$  parameter is positively correlated with the specific surface area of the pores and the volume of the micropores. This suggests that as  $D_2$  increases, the increase in micropore volume enhances the gas adsorption and storage capacity. Nonetheless, shale with a high  $D_2$  value features small pores and a complex structure, presenting challenges to gas transmission within the shale. In summary, the layers in the ORSS characterized by appropriately low  $D_1$  and high  $D_2$  are more conducive to natural gas accumulation and later development.

In the case of ORMS and ORAS,  $D_1$  exhibited a favorable association with both the specific surface area and volume of pores, as well as the clay content. This signifies that with an increase in  $D_1$ , the clay mineral content increases, offering a certain storage capacity but not favoring subsequent development.  $D_2$  displays a positive correlation with quartz content and is inversely related to pore size. An excessively elevated  $D_2$  value will impede the available space for free gas enrichment. Hence, for ORMS and ORAS, choosing suitably elevated values

of both  $D_1$  and  $D_2$  is more advantageous for gas enrichment and subsequent development. However, certain constraints should also be considered.

## VI. CONCLUSIONS

The Longmaxi Formation deep shale is mainly composed of ORSS and ORMS lithofacies. The main pore types are OM pores, microfractures, and dissolution pores. The pores in ORSS are controlled by TOC and quartz content, while those in ORMS and ORAS are controlled by TOC and clay content. Small-scale pores show relatively uniform characteristics, while larger pores exhibit complex and diverse features. The preservation of siliceous minerals and high pressure is the key to maintaining high-quality reservoirs in deep shale.

The pore systems of deep shale can be classified into three major categories: ultramicro adsorption pores, nano diffusion pores, and micro/nano flow-diffusion pores. The gas transport modes can be further subdivided into surface adsorption-diffusion, Knudsen diffusion, Fick diffusion, slip flow, and continuous flow. Among them, nano-scale OM pores are widely developed, and gas is mostly transported in the form of adsorption-diffusion. There is a lack of continuous flow spaces such as microfractures.

Micropores and mesopores are more abundant in deep shale than in shallow shale. They are mainly OM pores, dissolution pores, and clay mineral pores. The controlling effect of microfractures on the continuous flow of natural gas varies greatly between deep and shallow layers, which is also an important reason why it is difficult to achieve effective stimulation and stable production in deep shale. For the over-pressure areas below 3500 m in the basin, the Longmaxi Formation has prospects for resource exploration, especially those with ORSS of low  $D_1$  and high  $D_2$  value, as well as ORMS and ORAS of high  $D_1$  and high  $D_2$  value.

## ACKNOWLEDGMENTS

This research was supported by the National Natural Science Foundation of China (42372144). We extend our gratitude for the assistance provided by the China National Petroleum Corporation and acknowledge their authorization to publish the data.

## AUTHOR DECLARATIONS

### Conflict of Interest

The authors have no conflicts to disclose.

## Author Contributions

**Shijie He:** Conceptualization (lead); Data curation (lead); Formal analysis (lead); Methodology (lead); Writing – original draft (lead); Writing – review & editing (lead). **Pingping Li:** Methodology (equal); Project administration (equal); Writing – review & editing (equal). **Zhenxue Jiang:** Funding acquisition (equal); Project administration (equal). **Xianglu Tang:** Funding acquisition (equal); Methodology (equal); Project administration (equal).

## DATA AVAILABILITY

The data that support the findings of this study are available from the corresponding author upon reasonable request.

## REFERENCES

- <sup>1</sup>F. Hao, H. Y. Zou, and Y. C. Lu, "Mechanisms of shale gas storage: Implications for shale gas exploration in China," *AAPG Bull.* **97**(8), 1325–1346 (2013).
- <sup>2</sup>C. N. Zou, Z. Yang, J. X. Dai, D. Z. Dong, B. M. Zhang, Y. M. Wang, S. H. Deng, J. L. Huang, K. Y. Liu, C. Yang, G. Q. Wei, and S. Q. Pan, "The characteristics and significance of conventional and unconventional Sinian–Silurian gas systems in the Sichuan Basin, central China," *Mar. Pet. Geol.* **64**, 386–402 (2015).
- <sup>3</sup>S. K. Gao, D. Z. Dong, K. Tao, W. Guo, X. J. Li, and S. R. Zhang, "Experiences and lessons learned from China's shale gas development: 2005–2019," *J. Nat. Gas Sci. Eng.* **85**, 103648–103661 (2021); X. L. Tang, Z. X. Jiang, Y. Song, Q. Luo, Z. Li, G. Z. Wang, and X. M. Wang, "Advances on the mechanism of reservoir forming and gas accumulation of the Longmaxi Formation shale in Sichuan Basin, China," *Energy Fuels* **35**, 3972–3988 (2021).
- <sup>4</sup>G. R. Chalmers, R. M. Bustin, and I. M. Power, "Characterization of gas shale pore systems by porosimetry, pycnometry, surface area, and field emission scanning electron microscopy/transmission electron microscopy image analyses: Examples from the Barnett, Woodford, Haynesville, Marcellus, and Doig units," *AAPG Bull.* **96**, 1099–1119 (2012).
- <sup>5</sup>L. C. Burrows, F. Haeri, P. Cvetic, S. Sanguinito, F. Shi, D. Tapriyal, A. Goodman, and R. M. Enick, "A literature review of CO<sub>2</sub>, natural gas, and water-based fluids for enhanced oil recovery in unconventional reservoirs," *Energy Fuels* **34**, 5331–5380 (2020).
- <sup>6</sup>B. Bai, M. Elgmati, H. Zhang, and M. Z. Wei, "Rock characterization of Fayetteville shale gas plays," *Fuel* **105**, 645–652 (2013).
- <sup>7</sup>M. M. Labani, R. Rezaee, A. Saeedi, and A. A. Hinaei, "Evaluation of pore size spectrum of gas shale reservoirs using low pressure nitrogen adsorption, gas expansion and mercury porosimetry: A case study from the Perth and Canning Basins, Western Australia," *J. Pet. Sci. Eng.* **112**, 7–16 (2013).
- <sup>8</sup>Y. Li, Z. S. Wang, Z. J. Pan, X. L. Niu, Y. Yu, and S. Z. Meng, "Pore structure and its fractal dimensions of transitional shale: A cross-section from east margin of the Ordos Basin, China," *Fuel* **241**, 417–431 (2019).
- <sup>9</sup>S. Kumar, V. A. Mendhe, A. D. Kamble, A. K. Varma, D. K. Mishra, M. Bannerjee, J. Buragohain, and A. K. Prasad, "Geochemical attributes, pore structures and fractal characteristics of Barakar shale deposits of Mand-Raigarh Basin, India," *Mar. Pet. Geol.* **103**, 377–396 (2019).
- <sup>10</sup>S. Xu, Q. Y. Gou, F. Hao, B. Q. Zhang, Z. G. Shu, Y. B. Lu, and Y. Wang, "Shale pore structure characteristics of the high and low productivity wells, Jiaoshiba shale gas field, Sichuan Basin, China: Dominated by lithofacies or preservation condition?" *Mar. Pet. Geol.* **114**, 104211–104226 (2020).
- <sup>11</sup>R. M. Slatt and N. R. O'Brien, "Pore types in the Barnett and Woodford gas shales: Contribution to understanding gas storage and migration pathways in fine-grained rocks," *AAPG Bull.* **95**, 2017–2030 (2011).
- <sup>12</sup>M. Arif, M. Mahmoud, Y. Zhang, and S. Iglauer, "X-ray tomography imaging of shale microstructures: A review in the context of multiscale correlative imaging," *Int. J. Coal Geol.* **233**, 103641–103660 (2021).
- <sup>13</sup>N. Gupta, E. Fathi, and F. Belyadi, "Effects of nano-pore wall confinements on rarefied gas dynamics in organic rich shale reservoirs," *Fuel* **220**, 120–129 (2018).
- <sup>14</sup>S. Baek and I. Y. Akkutlu, "Mean free path of gas molecules in organic nano-channels using molecular simulations," *SPE J.* **24**(6), 2555–2573 (2019).
- <sup>15</sup>N. Kovalchuk and C. Hadjistassou, "Integrating micro-scale modelling with core measurements to improve natural gas production in shale gas reservoirs," *J. Pet. Sci. Eng.* **201**, 108446–108455 (2021).
- <sup>16</sup>C. M. Freeman, G. J. Moridis, and T. A. Blasingame, "A numerical study of microscale flow behavior in tight gas and shale gas reservoir systems," *Transp. Porous Media* **90**, 253–268 (2011).
- <sup>17</sup>Q. Gao, S. C. Han, Y. F. Cheng, Y. Li, C. L. Yan, and Z. Y. Han, "Apparent permeability model for gas transport through micropores and microfractures in shale reservoirs," *Fuel* **285**, 119086 (2021).
- <sup>18</sup>Z. Y. Shao, S. J. He, L. L. Hou, Y. C. Wang, C. Tian, X. X. Liu, Y. R. Zhou, M. Z. Hao, and C. Y. Lin, "Dynamic accumulation of the quaternary shale biogas in Sanhu Area of the Qaidam Basin, China," *Energies* **15**, 4593–4613 (2022).
- <sup>19</sup>D. Q. Jiang, P. P. Li, M. J. Zheng, Q. Chen, W. T. Xiong, and H. Y. Zou, "Impacts of different matrix components on multi-scale pore structure and

- reservoir capacity: Insights from the Jurassic Da'anzhai member in the Yuanba area, Sichuan Basin," *Energy Rep.* **9**, 1251–1264 (2023).
- <sup>20</sup>M. M. Meng, H. K. Ge, Y. H. Shen, W. M. Ji, and Z. J. Li, "Insight into water occurrence and pore size distribution by nuclear magnetic resonance in Marine Shale Reservoirs, Southern China," *Energy Fuels* **37**(1), 319–327 (2023).
  - <sup>21</sup>M. M. Meng, Y. X. Zhang, B. Yuan, Z. J. Li, and Y. Zhang, "Imbibition behavior of oil-saturated rock: Implications for enhanced oil recovery in unconventional reservoirs," *Energy Fuels* **37**(18), 13759–13768 (2023).
  - <sup>22</sup>M. M. Meng, Y. X. Zhang, B. Yuan, Z. J. Li, and Y. Zhang, "Effect of initial water saturation and water film on imbibition behavior in tight reservoirs using nuclear magnetic resonance technique," *Phys. Fluids* **36**(5), 056603 (2024).
  - <sup>23</sup>A. Tripathy, A. Kumar, V. Srinivasan, K. H. Singh, and T. H. Sing, "Fractal analysis and spatial disposition of porosity in major Indian gas shales using low-pressure nitrogen adsorption and advanced image segmentation," *J. Nat. Gas Sci. Eng.* **72**, 103009–103025 (2019).
  - <sup>24</sup>T. Wu and S. Wang, "A fractal permeability model for real gas in shale reservoirs coupled with Knudsen diffusion and surface diffusion effects," *Fractals* **28**, 2050017 (2020).
  - <sup>25</sup>H. Yu, H. Y. Xu, J. C. Fan, Y. B. Zhu, F. C. Wang, and H. A. Wu, "Transport of shale gas in microporous/nanoporous media: Molecular to pore-scale simulations," *Energy Fuels* **35**, 911–943 (2021).
  - <sup>26</sup>Y. Ma, O. H. Ardakani, N. N. Zhong, H. L. Liu, H. P. Huang, S. Larter, and C. Zhang, "Possible pore structure deformation effects on the shale gas enrichment: An example from the Lower Cambrian shales of the Eastern Upper Yangtze Platform, South China," *Int. J. Coal Geol.* **217**, 103349–103371 (2020).
  - <sup>27</sup>J. Li, H. Li, C. Yang, Y. J. Wu, Z. Gao, and S. L. Jiang, "Geological characteristics and controlling factors of deep shale gas enrichment of the Wufeng-Longmaxi formation in the Southern Sichuan Basin, China," *Lithosphere* **2022**, 4737801.
  - <sup>28</sup>B. Bottoms, A. Potra, J. R. Samuelsen, and S. R. Schutter, "Geochemical investigations of the Woodford–Chattanooga and Fayetteville Shales: Implications for genesis of the Mississippi Valley-type zinc-lead ores in the southern Ozark Region and hydrocarbon exploration," *AAPG Bull.* **103**(7), 1745–1768 (2019).
  - <sup>29</sup>D. Becerra, G. Henry, and S. Roger, "Characterizing the two principal rock types comprising the Woodford Shale resource play: Application to shale geomechanics," *Interpretation* **6**(1), SC67–SC84 (2018).
  - <sup>30</sup>H. Y. Huang, D. F. He, Y. Q. Li, J. Li, and L. Zhang, "Silurian tectonic-sedimentary setting and basin evolution in the Sichuan area, southwest China: Implications for palaeogeographic reconstructions," *Mar. Pet. Geol.* **92**, 403–423 (2018).
  - <sup>31</sup>W. T. Zeng, J. C. Zhang, W. L. Ding, S. Zhao, Y. Q. Zhang, Z. J. Liu, and K. Jiu, "Fracture development in Paleozoic shale of Chongqing area (South China). Part one: Fracture characteristics and comparative analysis of main controlling factors," *J. Asian Earth Sci.* **75**, 251–266 (2013).
  - <sup>32</sup>H. Y. Huang, D. F. He, D. Li, Y. Q. Li, W. K. Zhang, and J. J. Chen, "Geochemical characteristics of organic-rich shale, Upper Yangtze Basin: Implications for the Late Ordovician–Early Silurian orogeny in South China," *Palaeogeogr. Palaeoclimatol. Palaeoecol.* **554**, 109822–109848 (2020).
  - <sup>33</sup>Y. Wang, H. F. Cheng, Q. H. Hu, L. F. Liu, and L. W. Hao, "Diagenesis and pore evolution for various lithofacies of the Wufeng-Longmaxi shale, southern Sichuan Basin, China," *Mar. Pet. Geol.* **133**, 105251 (2021).
  - <sup>34</sup>J. Teng, B. Liu, M. Mastalerz, and J. Schieber, "Origin of organic matter and organic pores in the overmature Ordovician–Silurian Wufeng–Longmaxi Shale of the Sichuan Basin, China," *Int. J. Coal Geol.* **253**, 103970 (2022).
  - <sup>35</sup>S. Y. Shi, Y. P. Wang, C. S. Chen, J. Z. Liu, and P. A. Peng, "Influence of tectonic evolution processes on burial, thermal maturation and gas generation histories of the Wufeng–Longmaxi shale in the Sichuan Basin and adjacent areas," *Int. J. Coal Geol.* **295**, 104642 (2024).
  - <sup>36</sup>X. Bin, X. Li, Z. H. Zhao, and X. Fu, "Sedimentary tectonic pattern of Wufeng and Longmaxi Formations in the northern margin of Sichuan Basin, South China," *Int. Geol. Rev.* **64**(15), 2166–2185 (2022).
  - <sup>37</sup>Q. Q. Feng, N. S. Qiu, T. Borjigin, H. Wu, J. T. Zhang, B. J. Shen, and J. S. Wang, "Tectonic evolution revealed by thermo-kinematic and its effect on shale gas preservation," *Energy* **240**, 122781 (2022).
  - <sup>38</sup>Y. F. Li, T. W. Zhang, G. S. Ellis, and D. Y. Shao, "Depositional environment and organic matter accumulation of Upper Ordovician–Lower Silurian marine shale in the Upper Yangtze Platform, South China," *Palaeogeogr. Palaeoclimatol. Palaeoecol.* **466**, 252–264 (2017).
  - <sup>39</sup>C. N. Yan, Z. J. Jin, J. H. Zhao, W. Du, and Q. Y. Liu, "Influence of sedimentary environment on organic matter enrichment in shale: A case study of the Wufeng and Longmaxi Formations of the Sichuan Basin, China," *Mar. Pet. Geol.* **92**, 880–894 (2018).
  - <sup>40</sup>X. M. Wang, L. F. Liu, Y. Wang, Y. Sheng, S. S. Zheng, W. W. Wu, and Z. H. Luo, "Comparison of the pore structures of Lower Silurian Longmaxi Formation shales with different lithofacies in the southern Sichuan Basin, China," *J. Nat. Gas Sci. Eng.* **81**, 103419–103430 (2020).
  - <sup>41</sup>S. Brunauer, P. H. Emmett, and E. Teller, "Adsorption of gases in multimolecular layers," *J. Am. Chem. Soc.* **60**, 309–319 (1938).
  - <sup>42</sup>E. P. Barrett, L. G. Joyner, and P. P. Halenda, "The Determination of pore volume and area distributions in porous substances. I. Computations from Nitrogen Isotherms," *J. Am. Chem. Soc.* **73**, 373–380 (1951).
  - <sup>43</sup>D. Avnir and M. Jaroniec, "An isotherm equation for adsorption on fractal surfaces of heterogeneous porous materials," *Langmuir* **5**(6), 1431–1433 (1989).
  - <sup>44</sup>M. Jaroniec, "Evaluation of the fractal dimension from a single adsorption isotherm," *Langmuir* **11**(6), 2316–2317 (1995).
  - <sup>45</sup>Y. Feng, X. M. Xiao, P. Gao, E. Z. Wang, D. F. Hu, R. B. Liu, G. Li, and C. G. Lu, "Restoration of sedimentary environment and geochemical features of deep marine Longmaxi shale and its significance for shale gas: A case study of the Dingshan area in the Sichuan Basin, South China," *Mar. Pet. Geol.* **151**, 106186 (2023).
  - <sup>46</sup>X. L. Tang, Z. X. Jiang, H. X. Huang, S. Jiang, L. Yang, F. Y. Xiong, L. Cheng, and J. Feng, "Lithofacies characteristics and its effect on gas storage of the Silurian Longmaxi marine shale in the southeast Sichuan Basin, China," *J. Nat. Gas Sci. Eng.* **28**, 338–346 (2016).
  - <sup>47</sup>C. H. Ou, C. H. Li, Z. H. Rui, and Q. Ma, "Lithofacies distribution and gas-controlling characteristics of the Wufeng–Longmaxi black shales in the southeastern region of the Sichuan Basin, China," *J. Pet. Sci. Eng.* **165**, 269–283 (2018).
  - <sup>48</sup>R. G. Loucks, R. M. Reed, S. C. Ruppel, and D. M. Jarvie, "Morphology, genesis, and distribution of nanometer-scale pores in siliceous mudstones of the Mississippian Barnett shale," *J. Sediment Res.* **79**, 848–861 (2009).
  - <sup>49</sup>C. R. Clarkson, N. Solano, R. M. Bustin, A. M. M. Bustin, G. R. Chalmers, L. He, Y. B. Melnichenko, A. P. Radlinski, and T. P. Blach, "Pore structure characterization of North American shale gas reservoirs using USANS/SANS, gas adsorption, and mercury intrusion," *Fuel* **103**, 606–616 (2013).
  - <sup>50</sup>U. Kuila and M. Prasad, "Surface area and pore-size distribution in clays and shales," *Geophys. Prospect.* **61**, 341–362 (2013).
  - <sup>51</sup>R. Aringhieri, "Nanoporosity characteristics of some natural clay minerals and soils," *Clays Clay Miner.* **52**, 700–704 (2004).
  - <sup>52</sup>D. J. Ross and R. M. Bustin, "The importance of shale composition and pore structure upon gas storage potential of shale gas reservoirs," *Mar. Pet. Geol.* **26**, 916–927 (2009).
  - <sup>53</sup>W. M. Ji, T. W. Zhang, K. L. Milliken, J. L. Qu, and X. L. Zhang, "Experimental investigation of main controls to methane adsorption in clay-rich rocks," *Appl. Geochem.* **27**, 2533–2545 (2012).
  - <sup>54</sup>E. T. Baruch, M. J. Kennedy, S. C. Lohr, and D. N. Dewhurst, "Feldspar dissolution-enhanced porosity in Paleoproterozoic shale reservoir facies from the Barney Creek Formation (McArthur Basin, Australia)," *AAPG Bull.* **99**, 1745–1770 (2015).
  - <sup>55</sup>T. Topor, A. Derkowski, P. Ziemianski, J. Szczurowski, and D. K. McCarty, "The effect of organic matter maturation and porosity evolution on methane storage potential in the Baltic Basin (Poland) shale-gas reservoir," *Int. J. Coal Geol.* **180**, 46–56 (2017).
  - <sup>56</sup>L. T. Ko, S. C. Ruppel, R. G. Loucks, P. C. Hackley, T. W. Zhang, and D. Y. Shao, "Pore-types and pore-network evolution in Upper Devonian–Lower Mississippian Woodford and Mississippian Barnett mudstones: Insights from laboratory thermal maturation and organic petrology," *Int. J. Coal Geol.* **190**, 3–28 (2018).
  - <sup>57</sup>F. Yang, Z. F. Ning, and H. Q. Liu, "Fractal characteristics of shales from a shale gas reservoir in the Sichuan Basin, China," *Fuel* **115**, 378–384 (2014).
  - <sup>58</sup>A. Sakhaee-Pour and W. F. Li, "Fractal dimensions of shale," *J. Nat. Gas Sci. Eng.* **30**, 578–582 (2016).
  - <sup>59</sup>M. S. Rahner, M. Halisch, C. P. Fernandes, A. Weller, and V. S. S. D. Santos, "Fractal dimensions of pore spaces in unconventional reservoir rocks using X-ray nano- and micro-computed tomography," *J. Nat. Gas Sci. Eng.* **55**, 298–311 (2018).



- <sup>60</sup>C. D. Piane, H. Ansari, Z. S. Li, J. Mata, W. Rickard, R. Pini, D. N. Dewhurst, and N. Sherwood, "Influence of organic matter type on porosity development in the Wufeng-Longmaxi Shale: A combined microscopy, neutron scattering and physisorption approach," *Int. J. Coal Geol.* **249**, 103880 (2022).
- <sup>61</sup>W. M. Ji, F. Hao, Y. Song, J. Q. Tian, M. M. Meng, and H. X. Huang, "Organic geochemical and mineralogical characterization of the lower Silurian Longmaxi shale in the southeastern Chongqing area of China: Implications for organic matter accumulation," *Int. J. Coal Geol.* **220**, 103412 (2020).
- <sup>62</sup>Q. Z. Guan, D. Z. Dong, H. L. Zhang, S. S. Sun, S. R. Zhang, and W. Guo, "Types of biogenic quartz and its coupling storage mechanism in organic-rich shales: A case study of the Upper Ordovician Wufeng Formation to Lower Silurian Longmaxi Formation in the Sichuan Basin, SW China," *Pet. Explor. Dev.* **48**(4), 813–823 (2021).
- <sup>63</sup>H. Darabi, A. Etehad, F. Javadpour, and K. Sepehrnoori, "Gas flow in ultra-tight shale strata," *J. Fluid Mech.* **710**, 641–658 (2012).
- <sup>64</sup>R. Heller, J. Vermilyen, and M. Zoback, "Experimental investigation of matrix permeability of gas shales," *AAPG Bull.* **98**, 975–995 (2014).
- <sup>65</sup>K. L. Wu, Z. X. Chen, and X. F. Li, "Real gas transport through nanopores of varying cross-section type and shape in shale gas reservoirs," *Chem. Eng. J.* **281**, 813–825 (2015).
- <sup>66</sup>K. L. Wu, Z. X. Chen, X. F. Li, C. H. Guo, and M. Z. Wei, "A model for multiple transport mechanisms through nanopores of shale gas reservoirs with real gas effect–adsorption-mechanic coupling," *Int. J. Heat Mass Transfer* **93**, 408–426 (2016).
- <sup>67</sup>P. H. Nelson, "Pore-throat sizes in sandstones, tight sandstones, and shales," *AAPG Bull.* **93**, 329–340 (2009).
- <sup>68</sup>M. Mastalerz, A. Schimmelmann, A. Drobniak, and Y. Y. Chen, "Porosity of Devonian and Mississippian New Albany Shale across a maturation gradient: Insights from organic petrology, gas adsorption, and mercury intrusion," *AAPG Bull.* **97**, 1621–1643 (2013).
- <sup>69</sup>K. Q. Liu, M. Ostadhassan, J. Zhou, T. Gentzis, and R. Rezaee, "Nanoscale pore structure characterization of the Bakken shale in the USA," *Fuel* **209**, 567–578 (2017).
- <sup>70</sup>H. Yu, J. Chen, Y. B. Zhu, F. C. Wang, and H. A. Wu, "Multiscale transport mechanism of shale gas in micro/nano-pores," *Int. J. Heat Mass Transfer* **111**, 1172–1180 (2017).
- <sup>71</sup>Z. Q. Li, I. A. Oyediran, R. Q. Huang, F. Hu, T. T. Du, R. L. Hu, and X. Li, "Study on pore structure characteristics of marine and continental shale in China," *J. Nat. Gas Sci. Eng.* **33**, 143–152 (2016).
- <sup>72</sup>Z. Q. Li, X. Shen, Z. Y. Qi, and R. L. Hu, "Study on the pore structure and fractal characteristics of marine and continental shale based on mercury porosimetry, N<sub>2</sub> adsorption and NMR methods," *J. Nat. Gas Sci. Eng.* **53**, 12–21 (2018).
- <sup>73</sup>G. F. Li, Z. J. Jin, X. Li, P. Y. Zhang, X. P. Liang, R. Zhang, C. R. Li, D. Wang, and Y. Z. Hu, "Shallow burial shale gas accumulation pattern of the Wufeng–Longmaxi Formations in the northern Guizhou area, western Yangtze platform," *Geoenergy Sci. Eng.* **225**, 211683–211699 (2023).
- <sup>74</sup>X. W. Guo, Z. J. Qin, R. Yang, T. Dong, S. He, F. Hao, J. Z. Yi, Z. G. Shu, H. Y. Bao, and K. Y. Liu, "Comparison of pore systems of clay-rich and silica-rich gas shales in the lower Silurian Longmaxi Formation from the Jiaoshiba area in the eastern Sichuan Basin, China," *Mar. Pet. Geol.* **101**, 265–280 (2019).
- <sup>75</sup>K. Ma, B. Zhang, S. Y. Wen, X. Y. Lin, Y. Wang, and K. Yang, "Quantitative characterization and controlling factors of shallow shale reservoir in Taiyang Anticline, Zhaotong Area, China," *Minerals* **12**(8), 998–1016 (2022).
- <sup>76</sup>C. H. Fan, H. Li, S. X. Zhao, Q. R. Qin, Y. Fan, J. F. Wu, and J. Zhang, "Formation stages and evolution patterns of structural fractures in marine shale: Case study of the Lower Silurian Longmaxi Formation in the Changning area of the southern Sichuan Basin, China," *Energy Fuels* **34**(8), 9524–9539 (2020).
- <sup>77</sup>C. Chen, C. L. Mu, K. K. Zhou, W. Liang, X. Y. Ge, X. P. Wang, Q. Y. Wang, and B. S. Zheng, "The geochemical characteristics and factors controlling the organic matter accumulation of the Late Ordovician-Early Silurian black shale in the Upper Yangtze Basin, South China," *Mar. Pet. Geol.* **76**, 159–175 (2016).
- <sup>78</sup>J. X. Dai, C. N. Zou, S. M. Liao, D. Z. Dong, Y. Y. Ni, J. L. Huang, W. Wu, S. P. Huang, and G. Y. Hu, "Geochemistry of the extremely high thermal maturity Longmaxi shale gas, Southern Sichuan Basin," *Org. Geochem.* **74**, 3–12 (2014).